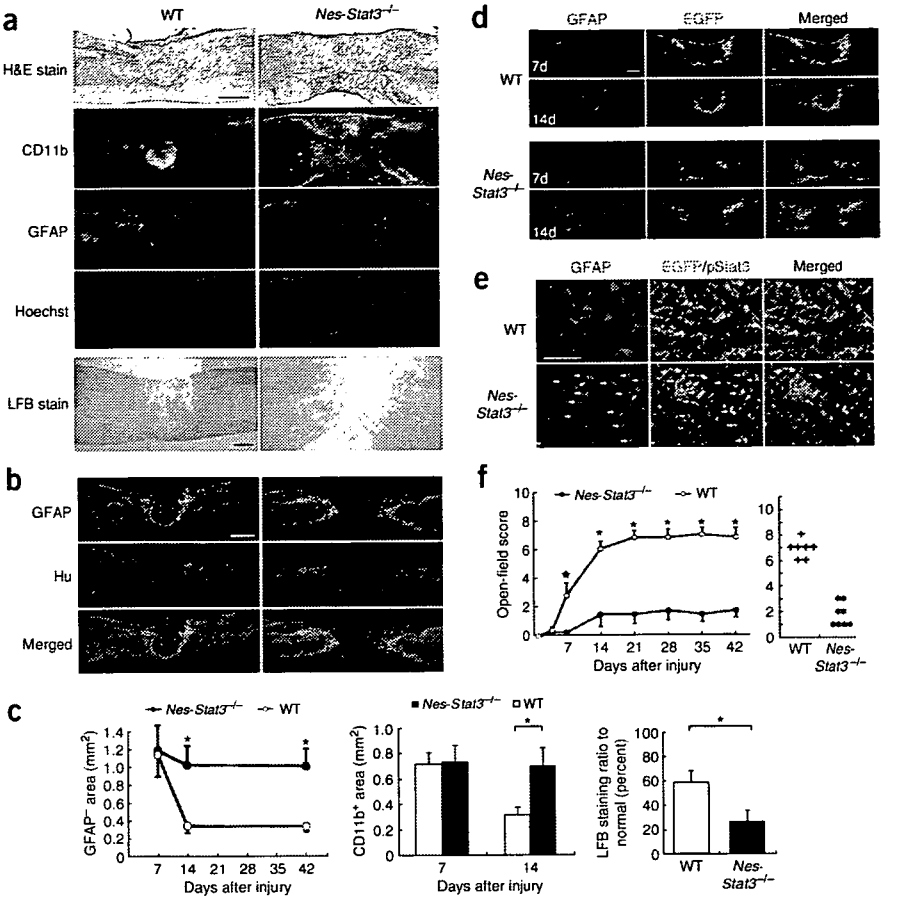

Figure 2 Compaction of inflammatory cells by reactive astrocytes and functional recovery were limited in *Nes-Stat3*$^{-/-}$ mice after SCI. **(a)** At 2 weeks after SCI, the infiltration of CD11b^{+} cells, GFAP^{-} area and demyelination were greater in *Nes-Stat3*$^{-/-}$ mice compared to wild-type (WT) littermates. Scale bars, 500 μm (upper left panel) and 300 μm (lower left panel). **(b)** The areas negative for Hu and GFAP were large in *Nes-Stat3*$^{-/-}$ mice even at 6 weeks after injury. Scale bar, 500 μm. **(c)** Comparison of GFAP^{-} area, CD11b^{+} area and LFB-positive area in both groups ($n = 3$ per each time point). Error bar indicates s.d. $^{*}P < 0.01$. **(d)** The location of GFAP^{+}EGFP^{+} reactive astrocytes shifted toward the lesion epicenter from 1 to 2 weeks in wild-type (WT) littermates, whereas their position remained relatively unchanged in *Nes-Stat3*$^{-/-}$ mice. Scale bar, 300 μm. **(e)** In *Nes-Stat3*$^{-/-}$ mice, Cre-mediated EGFP^{+} cells (green) were colocalized with GFAP^{+} reactive astrocytes (blue; arrows), but colocalization with phosphorylated Stat3 (red) was hardly observed at 4 d after injury. Scale bar, 100 μm. **(f)** Time course of functional recovery of lower limbs and the score of each mouse at 6 weeks after SCI. Whereas gradual recovery was observed in the subacute phase in wild-type (WT) littermates, little improvement was observed in *Nes-Stat3*$^{-/-}$ mice ($n = 7$ *Nes-Stat3*$^{-/-}$; $n = 8$ wild-type). Data are mean ± s.e.m. $^{*}P < 0.01$, $^{\star}P < 0.05$.

littermates and *Nes-Socs3*$^{-/-}$ mice became less pronounced at 2 weeks after injury, but *Nes-Socs3*$^{-/-}$ mice continually showed better motor function. Quantification of demyelination, oligodendrocyte-lost area and distal cord serotonergic innervation showed significant differences between the two groups (**Fig. 3f,h,i** and **Supplementary Fig. 4**). But GAP43^{+} regenerative fibers were comparable irrespective of genotype, and these fibers generally did not colocalize with 5HT^{+} fibers, indicating that the difference in serotonergic innervation did not result from regeneration (**Supplementary Fig. 5** online). These results suggest that the prompt contraction of the lesion spares more myelin, oligodendrocytes and serotonergic fibers, resulting in improved recovery.

Compared to wild-type mice, the development of reactive gliosis that secluded inflammatory cells was enhanced in *Nes-Socs3*$^{-/-}$ mice, whereas it was significantly delayed in *Nes-Stat3*$^{-/-}$ mice, indicating Stat3 signaling as an important factor in the developmental process of reactive gliosis after SCI (**Fig. 4a,b**).

Consistent with *in vivo* results, the *in vitro* migration behavior of astrocytes showed similar properties in a scratch-wounded assay that simulated the postinjury *in vivo* behavior of reactive astrocytes[17]. Astrocytes harvested from *Nes-Socs3*$^{-/-}$ mice showed a higher degree of migration, whereas impaired migration was observed in astrocytes of *Nes-Stat3*$^{-/-}$compared to wild-type mice (**Fig. 4c–e**). As proliferation rates among the three groups were comparable, cell migration activity was not dependent upon cell proliferation activity (data not shown).

A recent report indicates a possible molecular link between Stat3-zinc signaling and cell movement[18]. The zinc transporter LIV1, identified as the transcriptional downstream target of Stat3, was found to be essential for the nuclear localization of the zinc-finger protein Snail, a transcriptional repressor of the *Cdh1* gene (which encodes E-cadherin). Thus, the absence of Stat3 signaling causes dysregulation of cell adhesion and impairs cell movement. Strong support for this theory is given by the result that zinc deficiency impaired compaction of inflammatory cells by reactive astrocytes and increased the number of apoptotic cells after CNS injury[19]. In addition, CNS injury in knockout mice of metallothioneins (zinc-binding proteins involved in zinc ion regulation) had histological characteristics similar to *Nes-Stat3*$^{-/-}$ mice, such as impaired migratory behavior of reactive astrocytes, wide infiltration of inflammatory cells and severe impairment of wound healing[20]. On the other hand, astrocyte-targeted IL-6–expressing transgenic mice showed prompt migration of reactive astrocytes and compaction of inflammatory cells as well as substantial tissue repair after CNS injury[21] similar to *Nes-Socs3*$^{-/-}$ mice (though hyperactivation of IL-6 signaling without a specific cellular target caused considerably more damage owing to robust inflammation after CNS injury[6,22]). Here, expression of *Slc39a6* mRNA (encoding LIV1) in reactive astrocytes 5 d after injury was robust in wild-type mice but was limited in *Nes-Stat3*$^{-/-}$ mice. Consistent with *Slc39a6* mRNA expression, E-cadherin was expressed in reactive astrocytes of *Nes-Stat3*$^{-/-}$ but not in wild-type mice at 2 weeks after SCI. Furthermore, real-time RT-PCR of injured spinal cords showed differences in expression of *Scl39ac* mRNA among the three groups (**Fig. 4f–h**). These data provide insight into the mechanism of astrocytic migration through Stat3 signaling and indicate the significance of reactive astrocytes after CNS injury.

In our SCI model, the area of neuronal cell loss before the emergence of reactive astrocytes was comparable for wild-type and conditional knockout mice, suggesting that the effect of Stat3

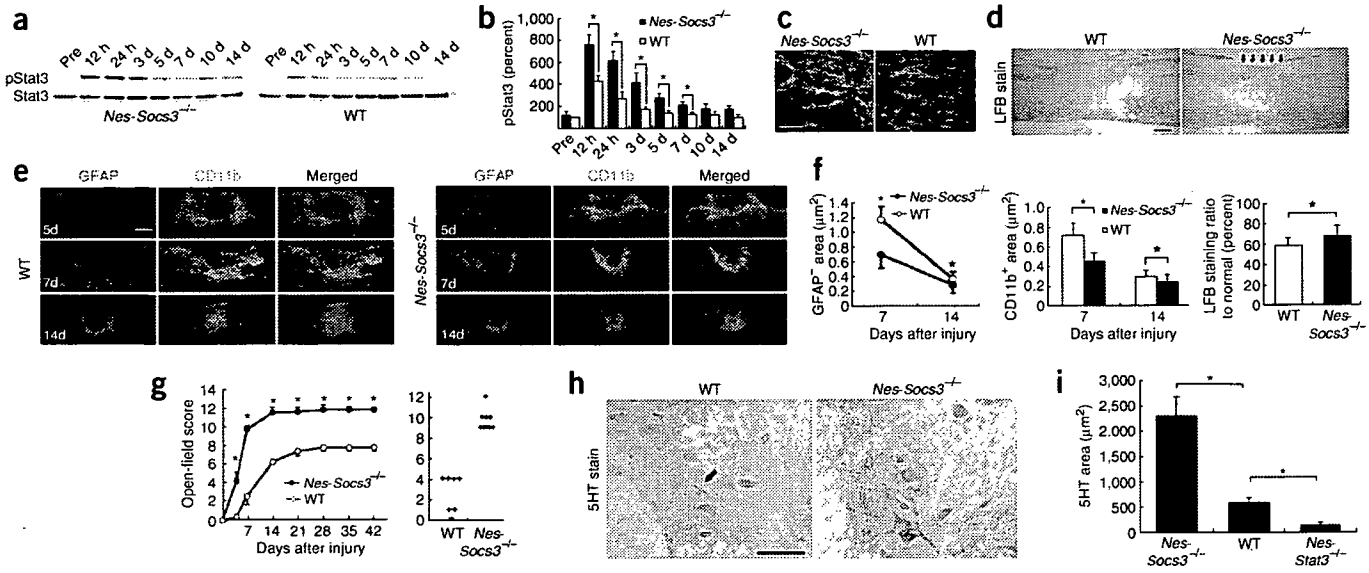

Figure 3 Enhanced activation of Stat3, prompt compaction of inflammatory cells and marked functional improvement in *Nes-Socs3*$^{-/-}$ mice. (**a**) Western blot analysis of Stat3 phosphorylation in injured spinal cord of wild-type (WT) and *Nes-Socs3*$^{-/-}$ mice. pStat3, phosphorylated Stat3. (**b**) Changes in the ratios of pStat3 to total Stat3 after SCI (mean ± s.e.m., $n = 4$ per group). $^{*}P < 0.05$. (**c**) Immunostaining of pStat3 and reactive astrocytes at 7 d after SCI. GFAP, red; pStat3, green. Scale bar, 100 μm. (**d**) Luxol Fast Blue (LFB) staining in littermates and *Nes-Socs3*$^{-/-}$ mice at 2 weeks after SCI. Arrows indicate the spared myelin in the dorsal part of the lesion epicenter. Scale bar, 300 μm. (**e**) Time course analysis of reactive astrocytes and CD11b^{+} cells. The early development of reactive astrocytes and compaction of inflammatory cells in *Nes-Socs3*$^{-/-}$ mice was visible as early as 7 d after SCI. Scale bar, 500 μm. (**f**) Quantitative analysis of GFAP^{-} area, CD11b^{+} area and LFB-positive area (mean ± s.d., $n = 4$). $^{*}P < 0.01$, $^{\star}P < 0.05$. (**g**) Time course of functional recovery and the score of each mouse at 7 d after SCI. Data are mean ± s.e.m. $^{*}P < 0.01$. (**h**) 5HT staining of the ventral horn distal to the lesion in wild-type (WT) littermates and *Nes-Socs3*$^{-/-}$ mice at 6 weeks after SCI. Arrow indicates spared 5HT^{+} fibers. Scale bar, 100 μm. (**i**) Quantitative analysis of serotonergic innervation of the distal cord in the three groups (mean ± s.e.m., $n = 4$ per each group). $^{*}P < 0.01$.

signaling on neuronal survival was minimal compared with its effect on the development and migration of reactive astrocytes (**Supplementary Fig. 1**).

The majority of studies on CNS injury have shown that the glial scar formed in part by reactive astrocytes hinders axonal regeneration. In mice lacking both GFAP and vimentin, reduced astroglial reactivity resulted in improved sprouting of axons and functional restoration after SCI[23]. But reactive astrocytes are also important for supporting repair of the blood-brain barrier. They prevent infiltration of CD45^{+} leukocytes and protect neurons and oligodendrocytes as shown by the selective ablation of dividing astrocytes using ganciclovir and GFAP-TK transgenic mice[24,25]. Here, we showed that Stat3 signaling in reactive astrocytes have a considerable role in the repair of injured tissue and the recovery of motor function. Although these results seem to conflict with one another, consideration of the timeframe in which these events were observed suggests a possible phase-dependent role of reactive astrocytes. In mice lacking both GFAP and vimentin, functional recovery was observed later than 2 weeks after injury[23], whereas substantial recovery was completed within 2 weeks after injury in *Nes-Stat3*$^{-/-}$ and *Nes-Socs3*$^{-/-}$ mice, suggesting that reactive astrocytes in the subacute phase repair tissue and restore function, whereas in the chronic phase of injury they impair axonal regeneration as a physical and chemical barrier.

Together, these results show that reactive astrocytes have a pivotal role in the repair of injured tissue and the recovery of motor function in the subacute phase after SCI, and that the function of reactive astrocytes is largely dependent on Stat3 signaling. This work also raises Stat3 signaling and reactive astrocytes as a potential new therapeutic target for the treatment of traumatic injury in CNS.

METHODS

Generation of conditional knockout mice. *Stat3*$^{loxP/loxP}$ mice, *Stat3*$^{loxP/-}$ mice, *Socs3*$^{loxP/loxP}$ mice, *Nes*-Cre mice and *CAG*-CAT$^{loxP/loxP}$–EGFP transgenic mice were as described elsewhere[3,11,12,14,15,26]. To generate *Nes-Stat3*$^{-/-}$ or *Nes-Socs3*$^{-/-}$ mice, we crossed *Nes*-Cre mice with *Stat3*$^{loxP/loxP}$, *Stat3*$^{loxP/-}$ mice[3,26] or *Socs3*$^{loxP/loxP}$ mice[15]. We used wild-type littermates (*Stat3*$^{loxP/loxP}$ or *Socs3*$^{loxP/loxP}$) as controls in histological and functional evaluations. We performed genotyping with primers described elsewhere[3,12,14,15]. All mice were housed in a temperature- and humidity-controlled environment on a 12-h light-dark cycle.

SCI model. We anesthetized adult C57BL/6J mice, wild-type littermates and conditional knockout mice (female, 8 weeks old) using an intraperitoneal injection of ketamine (100 mg/kg) and xylazine (10 mg/kg). After laminectomy at the tenth thoracic spinal vertebrae, we exposed the dorsal surface of the dura mater and induced SCI using a commercially available SCI device (60 kdyn using Infinite Horizon impactor, Precision Systems & Instrumentation) as previously described[27]. We evaluated motor function of the hind limbs with the locomotor rating test on the Basso-Beattie-Bresnahan (BBB) scale[28] for 6 weeks after injury. The obesity of *Nes-Stat3*$^{-/-}$ mice was not a problem in this study, because their functional recovery was limited to the point at which weight bearing was not an issue. All procedures were approved by the ethics committee of Keio University and were in accordance with the Guide for the Care and Use of Laboratory Animals (US National Institutes of Health).

Immunohistochemistry. We anesthetized mice and transcardially perfused them with 4% paraformaldehyde in 0.1 M PBS. We removed spinal cords, embedded them in OCT compound and sectioned them sagittally at 20 μm on a cryostat. We stained tissue sections with primary antibodies to GFAP (DAKO), cleaved caspase-3 (Cell Signaling), CD11b (a marker of monocyte/macrophages and granulocytes; MBL), BrdU (Chemicon), Nestin (Rat 401, Chemicon), GFP (MBL), phosphorylated Stat3 (Cell Signaling), GSTπ (BD Biosciences), serotonin (5HT; DiaSorin, Inc.), GAP43 (Chemicon), E-cadherin

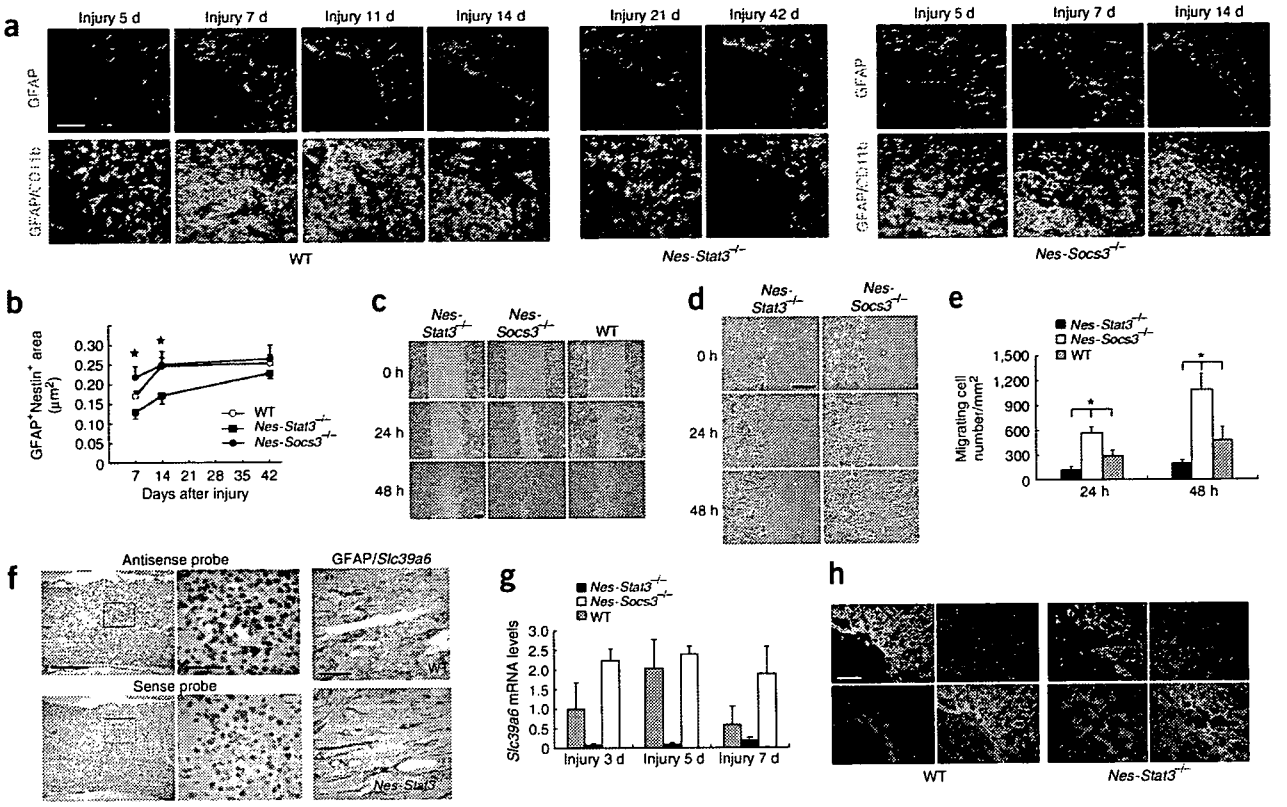

Figure 4 Involvement of Stat3 signaling in the development of reactive gliosis *in vivo*, the migration of reactive astrocytes *in vitro* and the transcriptional activity of LIV1. (**a**) Morphology of reactive astrocytes around the lesion area and infiltration of inflammatory cells in wild-type (WT), *Nes-Stat3*$^{-/-}$ and *Nes-Socs3*$^{-/-}$ mice. Scale bar, 100 μm. (**b**) The amount of reactive gliosis was measured as GFAP$^+$Nestin$^+$ (EGFP) area in the three groups ($n = 3$). Error bar indicates s.e.m. $^*P < 0.05$. (**c**) *In vitro* scratch injury of monolayer cultured astrocytes derived from wild-type (WT), *Nes-Stat3*$^{-/-}$ and *Nes-Socs3*$^{-/-}$ mice. Scale bar, 20 μm. (**d**) Magnified image of reactive astrocytes derived from *Nes-Stat3*$^{-/-}$ and *Nes-Socs3*$^{-/-}$ mice. Scale bar, 20 μm. (**e**) Migrating cells were quantified as mean number ± s.e.m. per millimeter squared beyond the wound edge ($n = 3$). $^*P < 0.01$. (**f**) *In situ* hybridization of *Slc39a6* mRNA in injured spinal cord. *Slc39a6* mRNA was observed in GFAP$^+$ reactive astrocytes in wild-type but was rarely found in *Nes-Stat3*$^{-/-}$ mice. Scale bars, 200 μm (upper left panel), 50 μm (upper middle panel) and 50 μm (upper right panel). (**g**) Expression of *Slc39a6* mRNA in injured spinal cords as determined by real-time RT-PCR in the three groups ($n = 3$). Each group was normalized to *Gapdh* values. There are significant differences ($P < 0.01$) among the three groups at each time point. Error bar indicates s.e.m. (**h**) Expression of E-cadherin (red) was not observed in reactive astrocytes of wild-type mice, whereas its active expression was observed in *Nes-Stat3*$^{-/-}$ mice at 2 weeks after SCI. GFAP, green; Hoechst stain, blue. Scale bar, 100 μm.

(Santa Cruz) and Hu[29] (a gift from R. Darnell, The Rockefeller University). We performed nuclear counterstaining with Hoechst 33342 (Molecular Probes). Images were obtained by fluorescence microscopy (Axioskop 2 Plus; Carl Zeiss) or confocal microscopy (LSM510; Carl Zeiss). To quantify the immunopositive and immunonegative area *in vivo*, we selected five representative midsagittal sections in each mouse and measured the area with the MCID system (Imaging Research, Inc.). We quantified the immunopositive area using grain counting and detected the immunonegative area by quantifying the dark area after image binarization. For myelin staining, we performed Luxol Fast Blue (LFB) stain. For comparison of LFB positive area, we selected five representative sagittal sections (3 mm long) of injured spinal cords (2 weeks after SCI) from positions 0.25 mm and 0.5 mm right of the midline, at the midline, and 0.25 mm and 0.5 mm left of the midline and LFB-positive area (blue area), and measured them by MCID system (grain counting), and calculated the ratio to normal section. To count GFAP$^+$BrdU$^+$ cells, we selected five representative sagittal sections and randomly captured six regions in each section at ×200 magnification by confocal microscopy. For quantification of 5HT$^+$ fibers, we randomly captured ten regions in each axial section of distal cord at ×200 magnification, and we quantified the total 5HT$^+$ area using the MCID system. We maintained light intensity and threshold values at constant levels for all analyses. In all sagittal sections shown here, the left side is rostral.

***In vitro* migration assay.** We prepared primary astrocytes from 2-d-old wild-type and conditional knockout mice as previously described[30]. After several passages in DMEM with 10% FBS, we trypsinized cells and plated them to confluency on coverslips coated with poly-L-lysine. After reaching subconfluency, we treated cells with 10 μg/ml mitomycin C for 2 h to avoid the effects of cell proliferation and then subjected them to scratching. We created a cell-free area by scratching the monolayer with a pipette tip and evaluated the migration of cells to the cell-free area from the surrounding area at 24 h and 48 h. We counted the number of migrating astrocytes after taking photographs of ten nonoverlapping fields.

Western blotting. We anesthetized SCI mice, transcardially perfused them with saline, and isolated and lysed a 4-mm long section of the injured spinal cord. We resolved lysates with SDS-PAGE and immunoblotted membranes with antibody to phosphorylated Stat3 (Tyr705) and antibody to Stat3 (Cell Signaling).

***In situ* hybridization.** For detection of *Slc39a6* mRNA, we subcloned a 774-bp DNA fragment corresponding to the nucleotide positions 331–1104 of mouse Slc39a6 into pGEMT-Easy vector (Promega) and used it to generate sense or antisense RNA probes. We hybridized paraffin-embedded spinal cord sections (6 μm) with digoxigenin-labeled RNA probes at 60 °C for 16 h. We detected the bound label using NBT-BCIP, an alkaline phosphate color substrate. We counterstained sections with Kernechtrot.

Real-time quantitative PCR. We isolated total RNA from the injured spinal cord (4 mm long) using the RNeasy Kit (Qiagen) and obtained cDNA by

reverse transcriptase reaction. For quantitative analysis of *Slc39a6* mRNA expression, we used the cDNA as a template in a TaqMan real-time PCR assay using the ABI Prism 7000 sequence detection system (Applied Biosystems) according to the manufacturer's protocol. We performed the amplification using the following primers: forward primer, 5′-TGAAGGCAGCACCAATAG CA-3′; reverse primer, 5′-GGCCTGGATGGTGATCATG-3′; and TaqMan probe, 5′-FAM-CGTCACTGAAATTGTGCAGCCCGTC-TAMRA-3′.

Statistical analysis. We performed statistical analysis with an unpaired two-tailed Student *t*-test for single comparisons, and ANOVA followed by the Tukey-Kramer test for multiple comparisons. For the open-field score, we used repeated-measures ANOVA and the Mann-Whitney *U*-test. In all statistical analyses, significance was accepted at $P < 0.05$.

Accession codes. GenBank: *Mus musculus* solute carrier family 39 (metal ion transporter) number 6 (Slc39a6), NM_139143.

Note: Supplementary information is available on the Nature Medicine website.

ACKNOWLEDGMENTS

This work was supported by grants from Ministry of Education, Culture, Sports, Science and Technology (MEXT), Japan, the General Insurance Association in Japan, Terumo Foundation Life Science Foundation (to H.O.), and a Grant-in-Aid for the 21st century COE program, Keio Gijuku Academic Development Funds.

AUTHOR CONTRIBUTIONS

S.O. performed most of the experiments to characterize mouse phenotypes. M.N. instructed group members about experimental processes. H.K. helped prepare the manuscript. T.M. and T.S. maintained and prepared knockout mice. K.I. and J.Y. prepared spinal cord–injured animals. A.Y. provided *Nes-Socs3*$^{-/-}$ mice. Y.I. advised experiments by S.O. Y.T. and H.O. designed experiments and prepared the manuscript.

COMPETING INTERESTS STATEMENT

The authors declare that they have no competing financial interests.

Published online at http://www.nature.com/naturemedicine/
Reprints and permissions information is available online at http://npg.nature.com/reprintsandpermissions/

1. Silver, J. & Miller, J.H. Regeneration beyond the glial scar. *Nat. Rev. Neurosci.* **5**, 146–156 (2004).
2. Wang, T. *et al.* Regulation of the innate and adaptive immune responses by Stat-3 signaling in tumor cells. *Nat. Med.* **10**, 48–54 (2004).
3. Sano, S. *et al.* Keratinocyte-specific ablation of Stat3 exhibits impaired skin remodeling, but does not affect skin morphogenesis. *EMBO J.* **18**, 4657–4668 (1999).
4. Hirano, T., Ishihara, K. & Hibi, M. Roles of STAT3 in mediating the cell growth, differentiation and survival signals relayed through the IL-6 family of cytokine receptors. *Oncogene* **19**, 2548–2556 (2000).
5. Sriram, K., Benkovic, S.A., Hebert, M.A., Miller, D.B. & O'Callaghan, J.P. Induction of gp130-related cytokines and activation of JAK2/STAT3 pathway in astrocytes precedes up-regulation of glial fibrillary acidic protein in the 1-methyl-4-phenyl-1,2,3,6-tetrahydropyridine model of neurodegeneration: key signaling pathway for astrogliosis *in vivo*? *J. Biol. Chem.* **279**, 19936–19947 (2004).
6. Kerr, B.J. & Patterson, P.H. Potent pro-inflammatory actions of leukemia inhibitory factor in the spinal cord of the adult mouse. *Exp. Neurol.* **188**, 391–407 (2004).
7. Xia, X.G., Hofmann, H.D., Deller, T. & Kirsch, M. Induction of STAT3 signaling in activated astrocytes and sprouting septal neurons following entorhinal cortex lesion in adult rats. *Mol. Cell. Neurosci.* **21**, 379–392 (2002).
8. Klein, M.A. *et al.* Impaired neuroglial activation in interleukin-6 deficient mice. *Glia* **19**, 227–233 (1997).
9. Frisen, J., Johansson, C.B., Torok, C., Risling, M. & Lendahl, U. Rapid, widespread, and longlasting induction of nestin contributes to the generation of glial scar tissue after CNS injury. *J. Cell Biol.* **131**, 453–464 (1995).
10. Johansson, C.B., Lothian, C., Molin, M., Okano, H. & Lendahl, U. Nestin enhancer requirements for expression in normal and injured adult CNS. *J. Neurosci. Res.* **69**, 784–794 (2002).
11. Takeda, K. *et al.* Stat3 activation is responsible for IL-6-dependent T cell proliferation through preventing apoptosis: generation and characterization of T cell-specific Stat3-deficient mice. *J. Immunol.* **161**, 4652–4660 (1998).
12. Betz, U.A., Vosshenrich, C.A., Rajewsky, K. & Muller, W. Bypass of lethality with mosaic mice generated by Cre-loxP-mediated recombination. *Curr. Biol.* **6**, 1307–1316 (1996).
13. Gao, Q. *et al.* Disruption of neural signal transducer and activator of transcription 3 causes obesity, diabetes, infertility, and thermal dysregulation. *Proc. Natl. Acad. Sci. USA* **101**, 4661–4666 (2004).
14. Kawamoto, S. *et al.* A novel reporter mouse strain that expresses enhanced green fluorescent protein upon Cre-mediated recombination. *FEBS Lett.* **470**, 263–268 (2000).
15. Mori, H. *et al.* Socs3 deficiency in the brain elevates leptin sensitivity and confers resistance to diet-induced obesity. *Nat. Med.* **10**, 739–743 (2004).
16. Kubo, M., Hanada, T. & Yoshimura, A. Suppressors of cytokine signaling and immunity. *Nat. Immunol.* **4**, 1169–1176 (2003).
17. Faber-Elman, A., Solomon, A., Abraham, J.A., Marikovsky, M. & Schwartz, M. Involvement of wound-associated factors in rat brain astrocyte migratory response to axonal injury: *in vitro* simulation. *J. Clin. Invest.* **97**, 162–171 (1996).
18. Yamashita, S. *et al.* Zinc transporter LIVI controls epithelial-mesenchymal transition in zebrafish gastrula organizer. *Nature* **429**, 298–302 (2004).
19. Penkowa, M., Giralt, M., Thomsen, P.S., Carrasco, J. & Hidalgo, J. Zinc or copper deficiency-induced impaired inflammatory response to brain trauma may be caused by the concomitant metallothionein changes. *J. Neurotrauma* **18**, 447–463 (2001).
20. Penkowa, M., Carrasco, J., Giralt, M., Moos, T. & Hidalgo, J. CNS wound healing is severely depressed in metallothionein I- and II-deficient mice. *J. Neurosci.* **19**, 2535–2545 (1999).
21. Penkowa, M. *et al.* Astrocyte-targeted expression of IL-6 protects the CNS against a focal brain injury. *Exp. Neurol.* **181**, 130–148 (2003).
22. Lacroix, S., Chang, L., Rose-John, S. & Tuszynski, M.H. Delivery of hyper-interleukin-6 to the injured spinal cord increases neutrophil and macrophage infiltration and inhibits axonal growth. *J. Comp. Neurol.* **454**, 213–228 (2002).
23. Menet, V., Prieto, M., Privat, A. & Gimenezy Ribotta, M. Axonal plasticity and functional recovery after spinal cord injury in mice deficient in both glial fibrillary acidic protein and vimentin genes. *Proc. Natl. Acad. Sci. USA* **100**, 8999–9004 (2003).
24. Bush, T.G. *et al.* Leukocyte infiltration, neuronal degeneration, and neurite outgrowth after ablation of scar-forming, reactive astrocytes in adult transgenic mice. *Neuron* **23**, 297–308 (1999).
25. Faulkner, J.R. *et al.* Reactive astrocytes protect tissue and preserve function after spinal cord injury. *J. Neurosci.* **24**, 2143–2155 (2004).
26. Ozawa, Y. *et al.* Downregulation of STAT3 activation is required for presumptive rod photoreceptor cells to differentiate in the postnatal retina. *Mol. Cell. Neurosci.* **26**, 258–270 (2004).
27. Scheff, S.W., Rabchevsky, A.G., Fugaccia, I., Main, J.A. & Lumpp, J.E., Jr. Experimental modeling of spinal cord injury: characterization of a force-defined injury device. *J. Neurotrauma* **20**, 179–193 (2003).
28. Basso, D.M., Beattie, M.S. & Bresnahan, J.C. Graded histological and locomotor outcomes after spinal cord contusion using the NYU weight-drop device versus transection. *Exp. Neurol.* **139**, 244–256 (1996).
29. Okano, H.J. & Darnell, R.B. A hierarchy of Hu RNA binding proteins in developing and adult neurons. *J. Neurosci.* **17**, 3024–3037 (1997).
30. Sanai, N. *et al.* Unique astrocyte ribbon in adult human brain contains neural stem cells but lacks chain migration. *Nature* **427**, 740–744 (2004).

nature medicine

A selective Sema3A inhibitor enhances regenerative responses and functional recovery of the injured spinal cord

Shinjiro Kaneko[1–3,9], Akio Iwanami[1,2,4,9], Masaya Nakamura[1], Akiyoshi Kishino[5], Kaoru Kikuchi[5], Shinsuke Shibata[2], Hirotaka J Okano[2], Takeshi Ikegami[1], Ayako Moriya[2], Osamu Konishi[5], Chikao Nakayama[5], Kazuo Kumagai[5], Toru Kimura[5], Yasufumi Sato[6], Yoshio Goshima[6], Masahiko Taniguchi[7], Mamoru Ito[8], Zhigang He[3], Yoshiaki Toyama[1] & Hideyuki Okano[2]

Axons in the adult mammalian central nervous system (CNS) exhibit little regeneration after injury. It has been suggested that several axonal growth inhibitors prevent CNS axonal regeneration. Recent research has demonstrated that semaphorin3A (Sema3A) is one of the major inhibitors of axonal regeneration. We identified a strong and selective inhibitor of Sema3A, SM-216289, from the fermentation broth of a fungal strain. To examine the effect of SM-216289 *in vivo*, we transected the spinal cord of adult rats and administered SM-216289 into the lesion site for 4 weeks. Rats treated with SM-216289 showed substantially enhanced regeneration and/or preservation of injured axons, robust Schwann cell–mediated myelination and axonal regeneration in the lesion site, appreciable decreases in apoptotic cell number and marked enhancement of angiogenesis, resulting in considerably better functional recovery. Thus, Sema3A is essential for the inhibition of axonal regeneration and other regenerative responses after spinal cord injury (SCI). These results support the possibility of using Sema3A inhibitors in the treatment of human SCI.

Several factors inhibit axonal regeneration after central nervous system (CNS) traumas such as spinal cord injury (SCI). Myelin-associated proteins, such as Nogo-A, myelin-associated glycoprotein (MAG) and oligodendrocyte-myelin glycoprotein (OMgp), have a central role in the inhibition of axonal regeneration[1–6]. Neutralization of Nogo receptor (NgR) signaling leads to marked axonal regeneration and functional recovery after SCI (ref. 7). In contrast, studies using Nogo knockout mice[8–10], NgR knockout mice[11,12] and other models[13–16] suggest that the blockade of axonal growth inhibitors other than myelin-associated proteins may also be important for axonal regeneration.

Among these factors, extracellular matrix molecules are likely to be important for the inhibition of axonal regrowth after SCI. CNS injury results in scar tissue formation at the injury site, which contains extracellular matrix molecules such as chondroitin sulphate proteoglycans (CSPGs)[17,18]. CSPGs are crucial as axonal growth inhibitors[17,18]: enzymatic degradation of CSPGs results in axonal regeneration and functional recovery[15]. Sema3A is another extracellular matrix molecule that may contribute to the inhibition of axonal regeneration[13,14,16] by acting on microtubules and the actin cytoskeleton[13,14,16,19–24]. In models of conditioning peripheral nerve injury, regenerating DRG axons halt selectively at Sema3A-enriched regions in the lesion site[14]. Thus, Sema3A may be a crucial extracellular factor that inhibits axonal regeneration after CNS injury. Neutralization of this molecule may hence lead to axonal regeneration and functional recovery after SCI. The high lethality of *Sema3a*$^{-/-}$ mice[22], however, has prevented close and large-scale genetic analyses of the contribution of Sema3A to the inhibitory environment of the injured spinal cord. An alternative method for large-scale analysis is to use a pharmacological approach.

Recently, we identified a small molecular agent, SM-216289, from a fungal extract, which can strongly inhibit Sema3A functions *in vitro*, including growth cone collapse and chemorepulsion of neurite extension[25,26]. SM-216289 strongly inhibits Sema3A functions *in vitro*[25,26] and SM-216289 acts directly on Sema3A to inhibit the binding of Sema3A to neuropilin-1 (NP-1), putatively by changing its steric structure. In this study, we investigated the action of SM-216289 in more detail and examined whether neutralizing Sema3A by administering SM-216289 to the injured spinal cord can create a more permissive environment for axonal regeneration *in vivo* or promote other regenerative responses, such as Schwann cell–mediated

[1]Department of Orthopaedic Surgery and [2]Department of Physiology, Keio University School of Medicine, 35 Shinanomachi, Shinjyuku-ku, Tokyo 160-8582, Japan. [3]Division of Neuroscience, Children's Hospital Boston, Harvard Medical School, 320 Longwood Avenue, Boston, Massachusetts 02115, USA. [4]Clinical Research Center, National Hospital Organization, Murayama Medical Center 2-37-1 Gakuen, Musashimurayama, Tokyo 208-0011, Japan. [5]Dainippon Sumitomo Pharma Co. Ltd., 3-1-98 Kasugade-naka, Konohana-ku, Osaka 554-0022, Japan. [6]Department of Molecular Pharmacology and Neurobiology, Yokohama City University School of Medicine, 3-9 Fukuura, Kanazawa-ku, Yokohama, Kanagawa 236-0004, Japan. [7]Department of Biochemistry, Tokyo University School of Medicine, 7-3-1 Hongo, Bunkyo-ku, Tokyo 113-0033, Japan. [8]Central Institute for Experimental Animals, 1430 Nogawa, Kawasaki, Kanagawa 216-0001, Japan. [9]These authors contributed equally to this work. Correspondence should be addressed to H.O. (hidokano@sc.itc.keio.ac.jp).

Received 24 October 2005; accepted 13 October 2006; published online 12 November 2006; doi:10.1038/nm1505

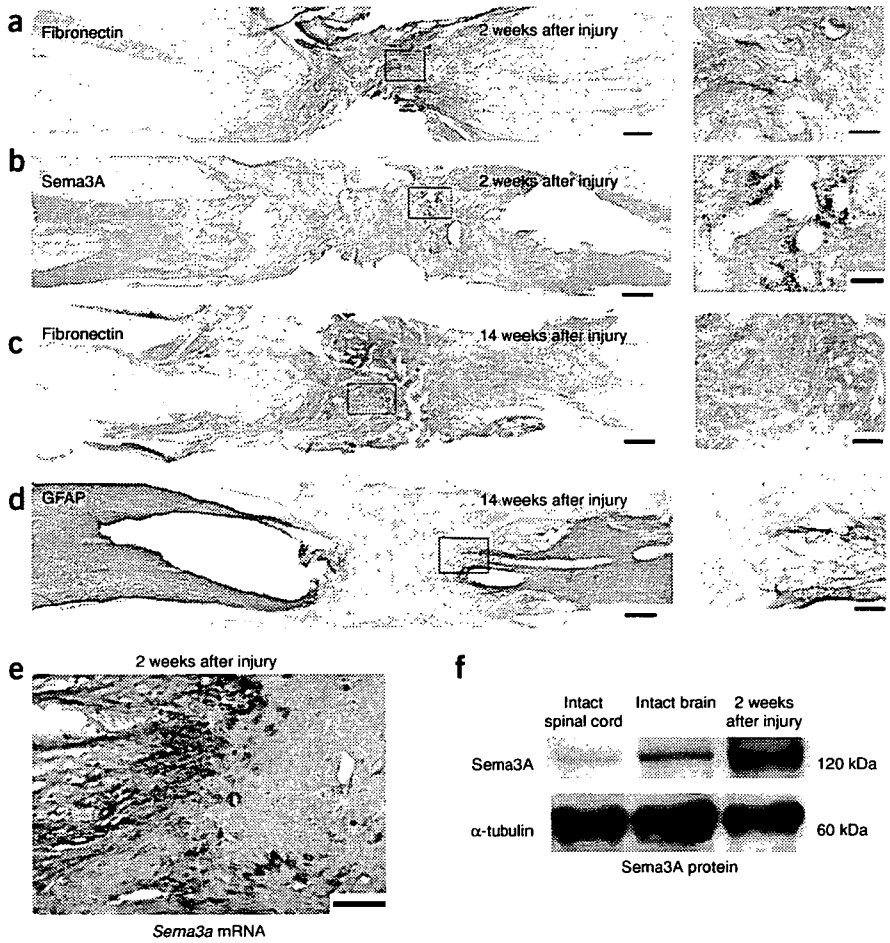

Figure 1 Expression of Sema3A after SCI. In all images, the left side is rostral. **(a–d)** Immunohistochemical analyses of the expression of fibronectin, Sema3A and GFAP in the transected spinal cord. Representative horizontal sections of the lesion site 2 weeks **(a,b)** and 14 weeks **(c,d)** after transection. Sections were stained with diaminobenzidine with nickel chloride (DAB nickel). Far right, magnified images of the boxed areas. Scale bars: 500 μm for left panels. 100 μm for right panels. **(e)** *Sema3a* mRNA expression in the lesion site 2 weeks after transection, as detected by *in situ* hybridization. Representative horizontal sections of the lesion site. Scale bar, 100 μm. **(f)** Sema3A protein expression in the lesion site as detected by immunoblotting.

myelination and axonal regeneration, inhibition of apoptosis and enhancement of angiogenesis. Our results support the potential of this Sema3A inhibitor as a therapeutic agent for human SCI patients.

RESULTS

Expression of Sema3A and other axonal growth inhibitors

In this study, we address the effect of a Sema3A inhibitor on axon regeneration in the injured spinal cord using a complete transection model. The transection model has the advantage of reproducibility, which permits a more accurate assessment of the effect of the treatment than other SCI models. Furthermore, the transection model is appropriate for the assessment of axonal regeneration. As a first step, we analyzed the spatiotemporal expression of Sema3A protein in the transected spinal cord. Two weeks after transection injury, we observed fibronectin-positive scar tissue at the lesion epicenter where Sema3A protein expression was also prominently detected (**Fig. 1a,b**). Also, 14 weeks after transection injury, the fibronectin-positive scar tissue, delineated by glial fibrillary acidic protein (GFAP)-positive glial scar tissues, extended more widely from the lesion epicenter than at 2 weeks after injury (**Fig. 1c,d**).

By *in situ* hybridization, it has been demonstrated that a marked induction of *Sema3a* mRNA takes place at the lesion site following SCI in both transection and contusion injuries[16]; *Sema3a* mRNA expression, detectable between 2 and 4 weeks after injury, was found to be colocalized with fibroblasts. Consistent with these results, we also detected high expression of *Sema3a* mRNA (by *in situ* hybridization) and Sema3A protein (by immunoblotting) (**Fig. 1e,f**). However, quantitative and temporal analyses of Sema3A protein expression after SCI have not been reported before. Therefore, we performed immunoblotting of spinal cord tissues harvested at several time points after SCI, in order to examine the temporal changes in the expression of Sema3A protein and other representative axonal growth inhibitors after spinal cord transection (**Fig. 2a–d**). We found that the expression of Sema3A protein within the transected spinal cord was upregulated at the lesion site with a peak between 1 and 2 weeks after the injury (**Fig. 2a,b**). The expression pattern of

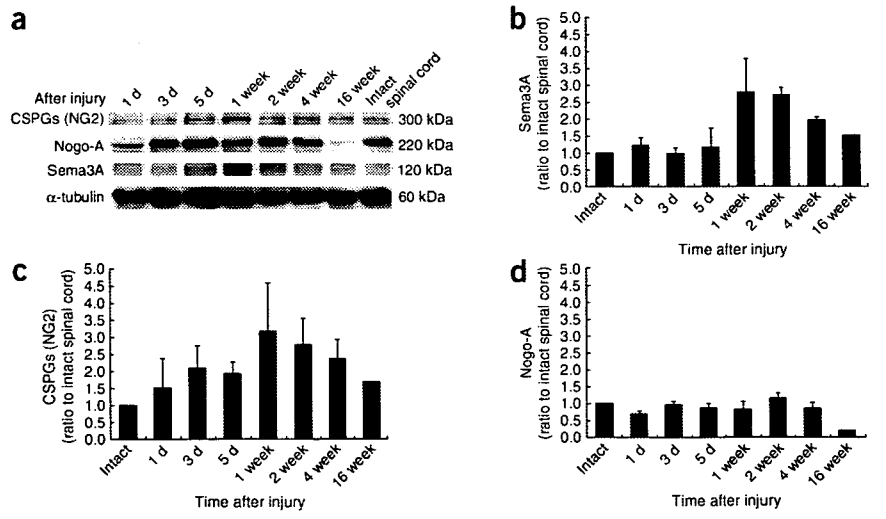

Figure 2 Temporal and quantitative analysis of Sema3A expression after SCI compared with the expression of other representative axonal growth inhibitors. **(a)** Temporal immunoblotting analysis. **(b–d)** Quantitative and temporal analysis. Data represent mean ± s.e.m.

NG2, which is representative of CSPGs upregulated after SCI, was temporally similar to that of Sema3A protein (**Fig. 2a,c**). In contrast, expression of Nogo-A, a representative myelin-associated protein, did not substantially increase within the transected spinal cord. Nogo-A expression was decreased at 16 weeks after injury, which may be partly attributable to demyelination of axons and phagocytosis of myelin debris (**Fig. 2a,d**).

Expression of NP-1 within the injured spinal cord

The receptor complex mediating Sema3A signals includes NP-1 (refs. 27–29) and plexins[30–32]. NP-1 has been reported to be the major component essential for Sema3A signaling and has a binding site for Sema3A. Therefore, we analyzed the spatiotemporal expression of NP-1 in the spinal cord after transection injury (**Supplementary Note** and **Supplementary Fig. 1** online). Considering the temporal expression patterns of Sema3A (**Fig. 2a,b**) and NP-1 (**Supplementary Fig. 1**) after injury, we administered the Sema3A inhibitor SM-216289 for 4 weeks after transection using an osmotic mini-pump (Alzet) in all subsequent experiments.

Strength and selectivity of the Sema3A inhibitor

As demonstrated previously[25,26], SM-216289 exerts a strong inhibitory effect on Sema3A. By screening various types of compounds (approximately 140,000) by growth cone collapse assay and collagen coculture assay using embroynic day (E) 7 or 8 chick DRG, we found that this compound has a maximal inhibitory effect on Sema3A. We compared SM-216289 with the tyrosine kinase inhibitor lavendustin A and the Cdk inhibitor olomoucine, which exert an inhibitory effect on Sema3A by acting intracellularly at the post-receptor level[23] (**Fig. 3a,b**). SM-216289 had a much stronger inhibitory effect on Sema3A than did either lavendustin A or olomoucine. In growth cone collapse assays, lavendustin A and olomoucine produced a minimal, if any, blockade of Sema3A-induced collapse at 1 U/ml, but not at 10 U/ml (**Fig. 3b**). In coculture assays in collagen gel, lavendustin A and olomoucine proved to have toxic effects on axonal extension at higher concentrations, unlike SM-216289 (**Fig. 3a**).

To elucidate whether SM-216289's action is selective for Sema3A, we examined (using a growth cone collapse assay) whether SM-216289 can inhibit the function of other representative axonal growth

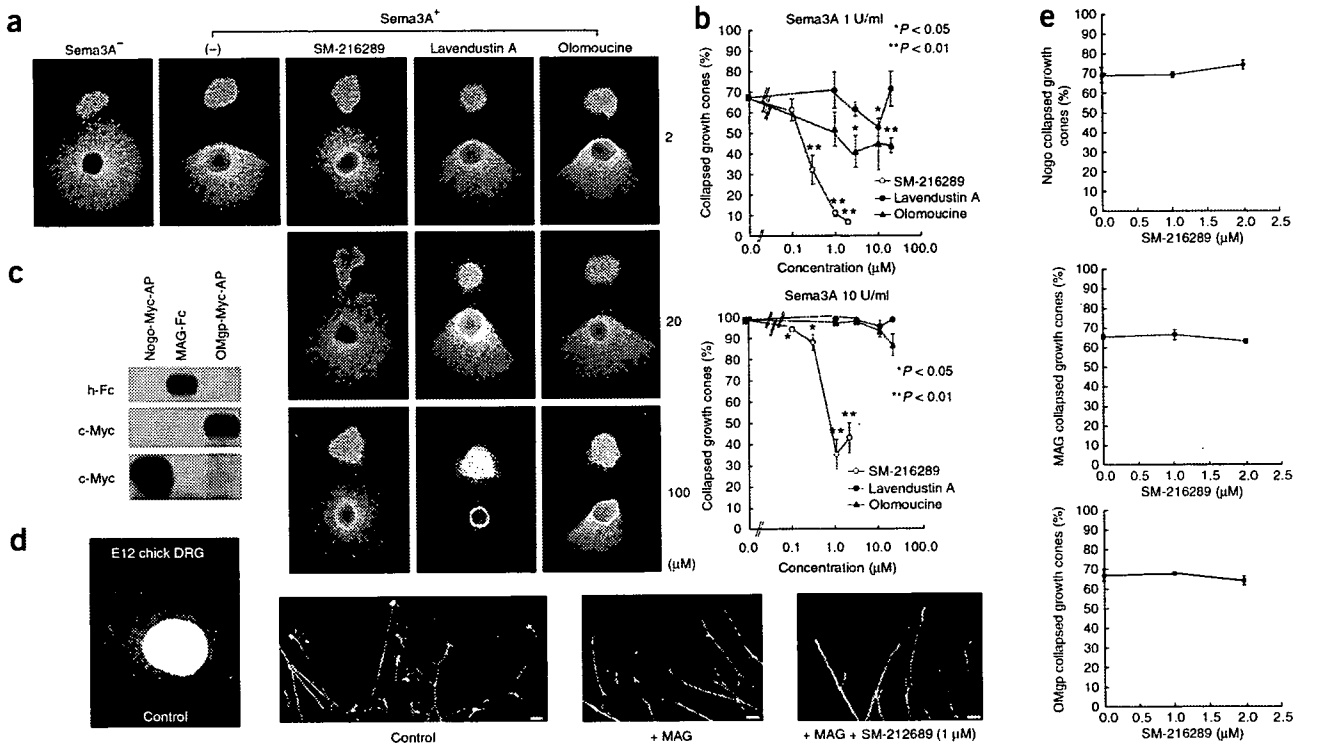

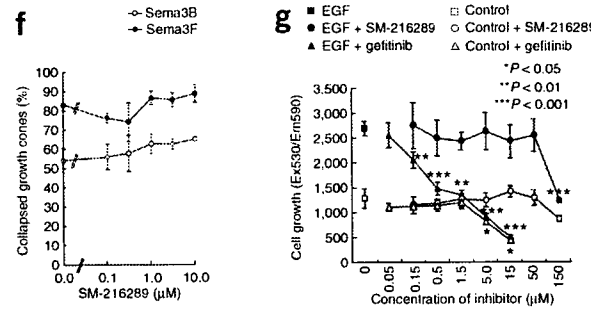

Figure 3 SM-216289 is a strong and specific Sema3A inhibitor. (**a**) Collagen coculture assay using embryonic day 8 (E8) chick DRG and Sema3A-expressing COS7 cell aggregates. SM-216289 and other compounds known to have an inhibitory effect on Sema3A, lavendustin A and olomoucine[23] were added at the indicated concentrations. (–), Sema3A with no additional compounds. (**b**) Effect of SM-216289, lavendustin A and olomoucine on growth cone collapse—induced by mouse Sema3A (1 U/ml or 10 U/ml)—in cultured E8 chick DRG. (**c**) The expression of Nogo-66-Myc-AP, MAG-Fc and OMgp-Myc-AP after transfection into HEK293T cells was confirmed by immunoblotting. (**d**) Growth cone collapse assay using E12 chick DRG. Left two panels, control growth cones. Right two panels, growth cones after incubation with MAG, with or without SM-216289. Scale bars, 20 μm. (**e**) Rate of growth cone collapse after incubation in the presence of Nogo, MAG and OMgp, and various concentrations of SM-216289. (**f**) Rate of growth cone collapse after incubation in the presence of Sema3B and Sema3F with SM-216289. (**g**) Cell growth assay using KB cells with growth dependent on epidermal growth factor (EGF). Statistical analysis: Mann-Whitney *U*-test (**a–f**) or Student's *t*-test (**g**; compared with the respective no-drug samples). Data represent mean ± s.e.m. for **b,e,f**; mean ± s.d. for **g**.

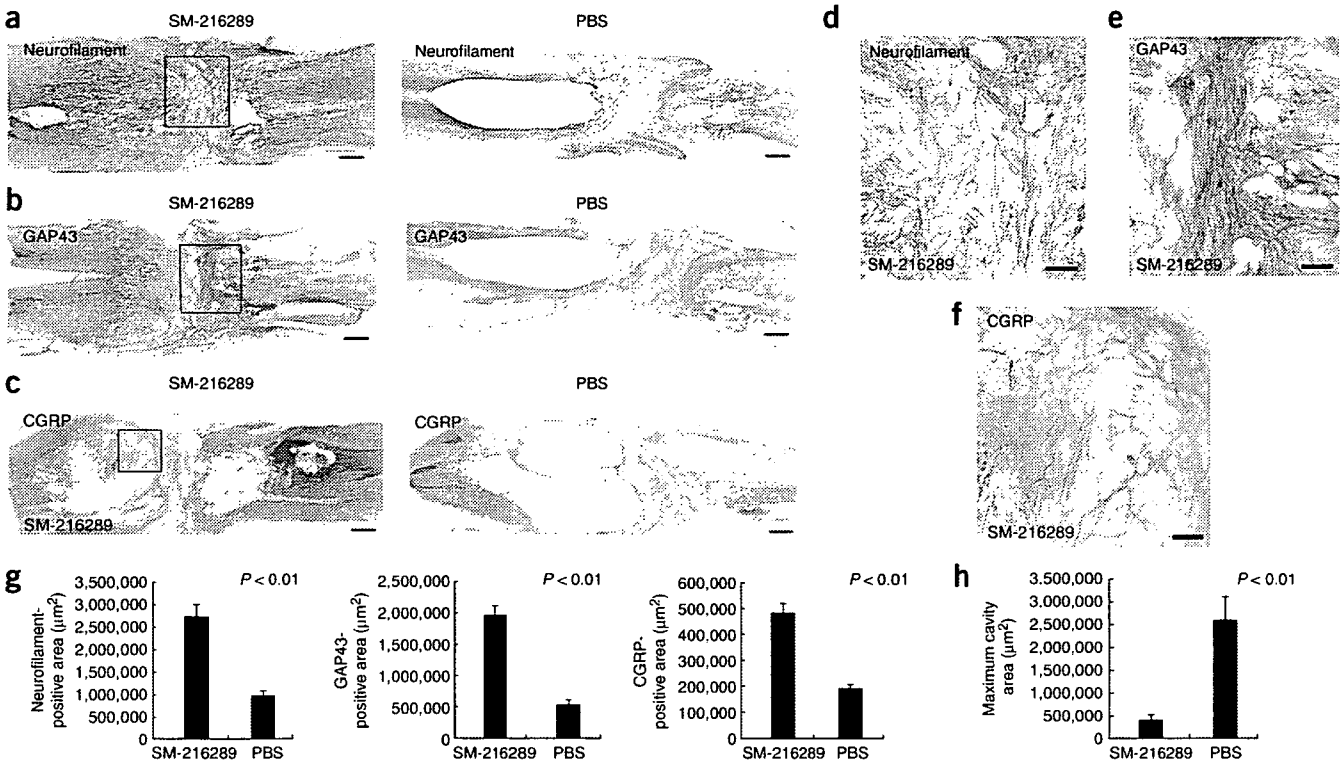

Figure 4 SM-216289 enhances axonal regeneration and reduces cavity volume in the injured spinal cord. (**a–c**) Immunohistochemical analyses of neurofilament (RT97), GAP43 and CGRP expression in the transected spinal cord. Representative horizontal sections of the lesion site 14 weeks after transection. Scale bars, 500 μm. (**d–f**) Magnified images of the boxed areas in **a–c**. The left side is rostral. Sections were stained with DAB nickel. Scale bars: 250 μm for **d,e**; 150 μm for **f**. (**g**) Quantitative analysis of the expression of neurofilament (RT97), GAP43 and CGRP in the transected spinal cord 14 weeks after spinal cord transection. (**h**) Quantitative analysis of the maximal dimension of the cavity area in the transected spinal cord 14 weeks after spinal cord transection. Sections were stained with DAB nickel. Statistical analysis was performed using the Mann-Whitney *U*-test. Data represent mean ± s.e.m.

inhibitors such as Nogo-A, MAG and OMgp, as well as other Sema3 family members, including Sema3B and Sema3F (ref. 20) (**Fig. 3c–f**). To prepare soluble AP-Nogo-66-Myc, MAG-Fc, AP-OMgp-Myc, Sema3A-His, AP-Sema3B and AP-Sema3F proteins, we transfected the expression plasmids into HEK293T cells and confirmed the production of these proteins in supernatants from transfected HEK293T cells by immunoblotting analysis (**Fig. 3c**). We found SM-216289 to have almost no effect on growth cone collapse induced by Nogo-66, MAG or OMgp (**Fig. 3d,e**). In addition, SM-216289 did not show any effect on the response to Sema3B and Sema3F, type-3 semaphorins related to Sema3A in sympathetic ganglia (**Fig. 3f**), demonstrating that the blockade of Sema3A by this compound is highly specific.

We examined the pharmacological profile of SM-216289 in further detail. We obtained half-maximal inhibitory concentration (IC_{50}) values for receptor and ion channel binding assays, and enzyme and kinase inhibition tests (**Supplementary Table 1** online). Overall, these IC_{50} values were much higher than the values for Sema3A (**Supplementary Table 1**). SM-216289 (30 μM) also demonstrated no agonist activity toward the receptors (data not shown).

In addition, we also used cell growth assays to determine whether SM-216289 can affect intracellular signaling pathways (**Fig. 3g**). KB cells, whose growth is dependent on epidermal growth factor (EGF), were incubated for 3 d with SM-216289 or gefitinib ('Iressa'; an EGF receptor (EGFR) inhibitor) in the absence or presence of EGF (10 ng/ml). After incubation, cell growth was measured using Alamar Blue reagent (Trek Diagnostic Systems). Both SM-216289 (0.78 μM) and gefitinib (0.02–0.08 μM) inhibited the kinase activity of EGFR in a cell-free system. Gefitinib inhibited cell growth at a range of IC_{50} values corresponding to IC_{50} values of gefitinib. In contrast, EGF-dependent cell growth was significantly affected by SM-216289 only at concentrations much higher than those required for kinase inhibition *in vitro* (**Fig. 3g**; $P < 0.01$ at 150 μM). From this cell-based assay and the profiling data (**Supplementary Table 1**), we concluded that, at expected concentrations, SM-216289 at the lesion site after drug administration has almost no cell growth– or cell function–altering effects on ion channels, receptors, intracellular signaling pathways or gene transcription in injured neurons (**Supplementary Table 1** and **Fig. 3g**). These data indicate that SM-216289 is a strong, selective agent inhibiting Sema3A and thus an excellent molecular probe for investigating the mechanism underlying Sema3A function.

We also found that SM-216289 has a strong inhibitory effect on Sema3A *in vivo* as well as *in vitro* (**Supplementary Note** and **Supplementary Fig. 2** online).

SM-216289 enhances regeneration of injured axons

To examine the effect of a degradation in Sema3A-mediated signaling on the injured axons, we administered SM-216289 into the transected spinal cords of adult rats and performed immunohistochemical analyses 14 weeks after transection using specific markers. Given that Sema3A expression in the transected spinal cord mainly lasts up to 4 weeks after injury (**Fig. 2a,c**), we administered SM-216289 or PBS for 4 weeks using an osmotic mini-pump (Alzet). By inserting the

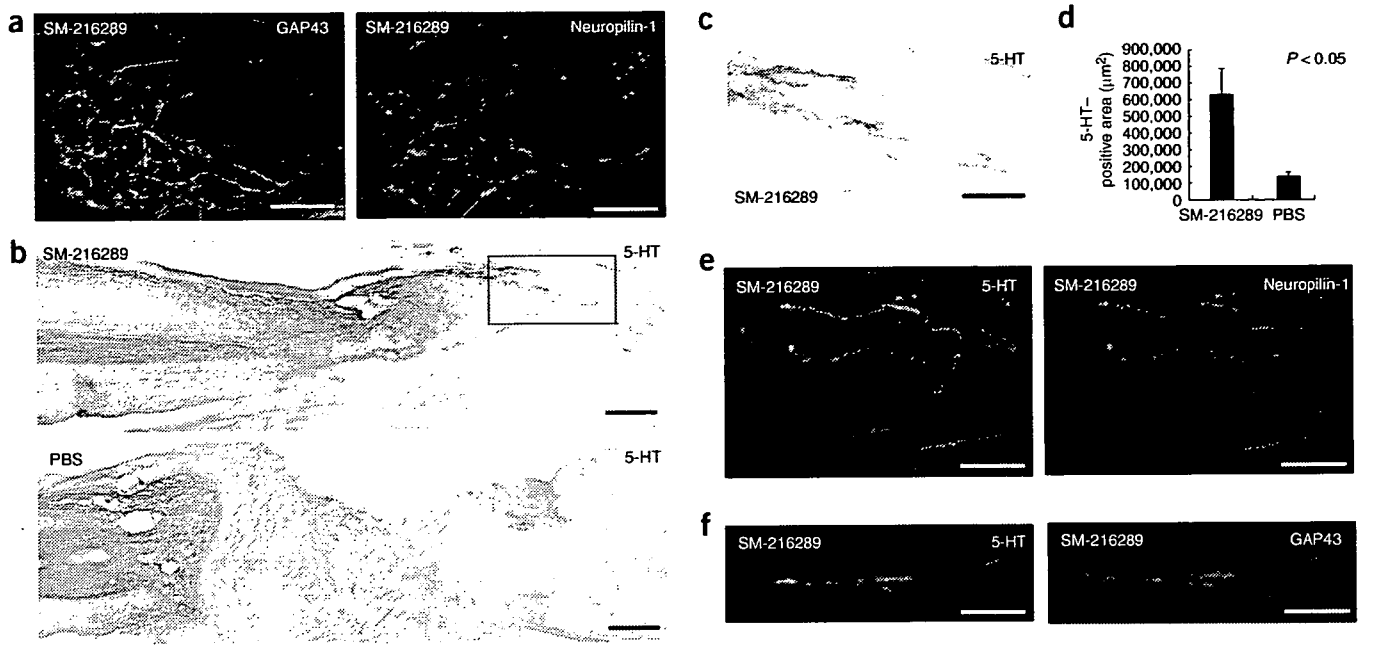

Figure 5 SM-216289 enhances axonal regeneration of NP-1–positive axons, including serotonergic (5-HT–positive) raphespinal tract axons, in the injured spinal cord. In all images, the left side is rostral. **(a)** Double-staining, in the transected spinal cord, with GAP43 and NP-1. Representative horizontal sections of the lesion site in SM-216289–administered rat. **(b)** Immunohistochemical analyses of serotonergic (5-HT–positive) raphespinal tract axons in the transected spinal cord. Representative horizontal sections of the lesion site 14 weeks after transection in SM-216289–administered and PBS-administered rats. Sections were stained with DAB nickel. **(c)** Magnified image of the boxed areas in **b**. **(d)** Quantitative analysis of expression of 5-HT in the transected spinal cord 14 weeks after spinal cord transection. **(e)** Double-staining with 5-HT and NP-1 in the transected spinal cord. Representative horizontal sections of the lesion site in SM-216289–administered rat. **(f)** Double-staining with 5-HT and GAP43 in the transected spinal cord. Representative horizontal sections of the lesion site in SM-216289–administered rat. Scale bars: 100 μm in **a,c,e,f**; 500 μm in **b**.

mini-pump tube just above the lesion epicenter, we ensured that SM-216289 had direct access to the lesion site. Using immunohistochemical analyses (**Fig. 4a–h**), we observed only a small number of neurofilament-positive axons within the lesion site in the control group, most probably the result of degenerative responses such as retractions. In contrast, we observed significantly more neurofilament-positive axons at the lesion site in the SM-216289–administered rats ($P < 0.01$; **Fig. 4a,d,g**). Moreover, we detected significantly more growth-associated protein 43 (GAP43)-positive axons within the lesion site in SM-216289–administered rats than in controls ($P < 0.01$; **Fig. 4b,e,g**). As GAP43 is a marker for regenerating axons, our findings suggest more robust axonal regeneration within the lesion site in the SM-216289–administered rats as compared with controls. Furthermore, most of the GAP43-positive axons expressed NP-1, suggesting that these axons can respond to both Sema3A and SM-216289 (**Fig. 5a**). However, it is also possible that the observed phenotypes resulting from the administration of SM-216289 are due to the enhanced preservation of injured axons. We next decided to characterize the axons in the lesion site more extensively. The sprouting of peptidergic nociceptive C fibers within the spinal cord after injury enhances several debilitating responses, such as neuropathic pain and autonomic dysreflexia[33]. We used a representative marker for these C-fiber axons, calcitonin gene–related peptide (CGRP), and observed significantly more CGRP-positive axons at the lesion site of SM-216289–administered rats as compared to controls ($P < 0.01$). However, the number of CGRP-positive neurons was very limited overall when compared with neurofilament-positive or GAP43-positive axons in the lesion site (less than one-fourth; **Fig. 4c,f,g**). Furthermore, previous reports have indicated that the abnormal sensory functions primarily result from the sprouting of uninjured CGRP-positive axons rather than injured CGRP-positive axons[34,35]. Considering the nature of the transection model in our experiment, most of the CGRP-positive axons we observed were most probably injured axons that had regenerated. However, there may have been some CGRP-positive axons adjacent to the lesion site that had not been transected, because CGRP-positive axons could originate from dorsal roots that enter the spinal cord rostral to the lesion site. To avoid including such uninjured axons, we counted axons only within the lesion site. In addition, paw withdrawal tests[34,35] did not show any allodynia (data not shown), suggesting that SM-216289 treatment is not likely to induce abnormal sensory function in this model. Parvalbumin (PV)-positive neurons are known to be proprioceptive sensory neurons, and it is possible that these neurons may have additional beneficial effects on behavioral function. By double-immunostaining for GAP43 and PV, we observed PV-positive axons among the regenerated axons (**Supplementary Fig. 3** online). However, the overall number of both CGRP-positive and PV-positive axons was limited, indicating that sensory neurons are not likely to be the major population among the regenerated axons. We did not observe the regeneration of ascending dorsal column axons (**Supplementary Fig. 3**) or the descending corticospinal tract (CST) through the lesion site in SM-216289–administered rats, consistent with the results from *Sema3a*$^{-/-}$ mice (data not shown). Notably, although we did not observe robust regeneration of serotonergic (that is, 5-hydoxytryptamine (5-HT)-positive) descending raphespinal tract axons[11,36] in the spinal cord in locations far caudal to the lesion site, 5-HT–positive axons appeared to cross the lesion site quite abundantly (inside the scar tissue) in the SM-216289–administered group (**Fig. 5b–d**). We

also confirmed that these serotonergic (5-HT–positive) raphespinal tract axons at the lesion site in the SM-216289–administered group expressed NP-1 (**Fig. 5e**) and GAP43 (**Fig. 5f**).

SM-216289 enhances Schwann cell migration

We also performed electron microscopic and immunohistochemical analyses to examine whether the regenerated axons become myelinated (**Fig. 6a,b**). We observed that most of the regenerated axons were myelinated in rats administered SM-216289, which was rarely seen in control rats (**Fig. 6b**). Notably, the myelination of the regenerated axons seemed to be of the peripheral type, which is characterized by the presence of Schwann cells, perineuria and basal lamina. This peripheral-type myelination indicates that Schwann cells migrate into the lesion site[37–39], and that these cells contributed to the myelination of regenerating fibers more extensively in the SM-216289–administered rats than in control rats. Therefore, we performed immunohistochemistry against P0, a representative marker of Schwann cells[40], and confirmed that migrated Schwann cells exist

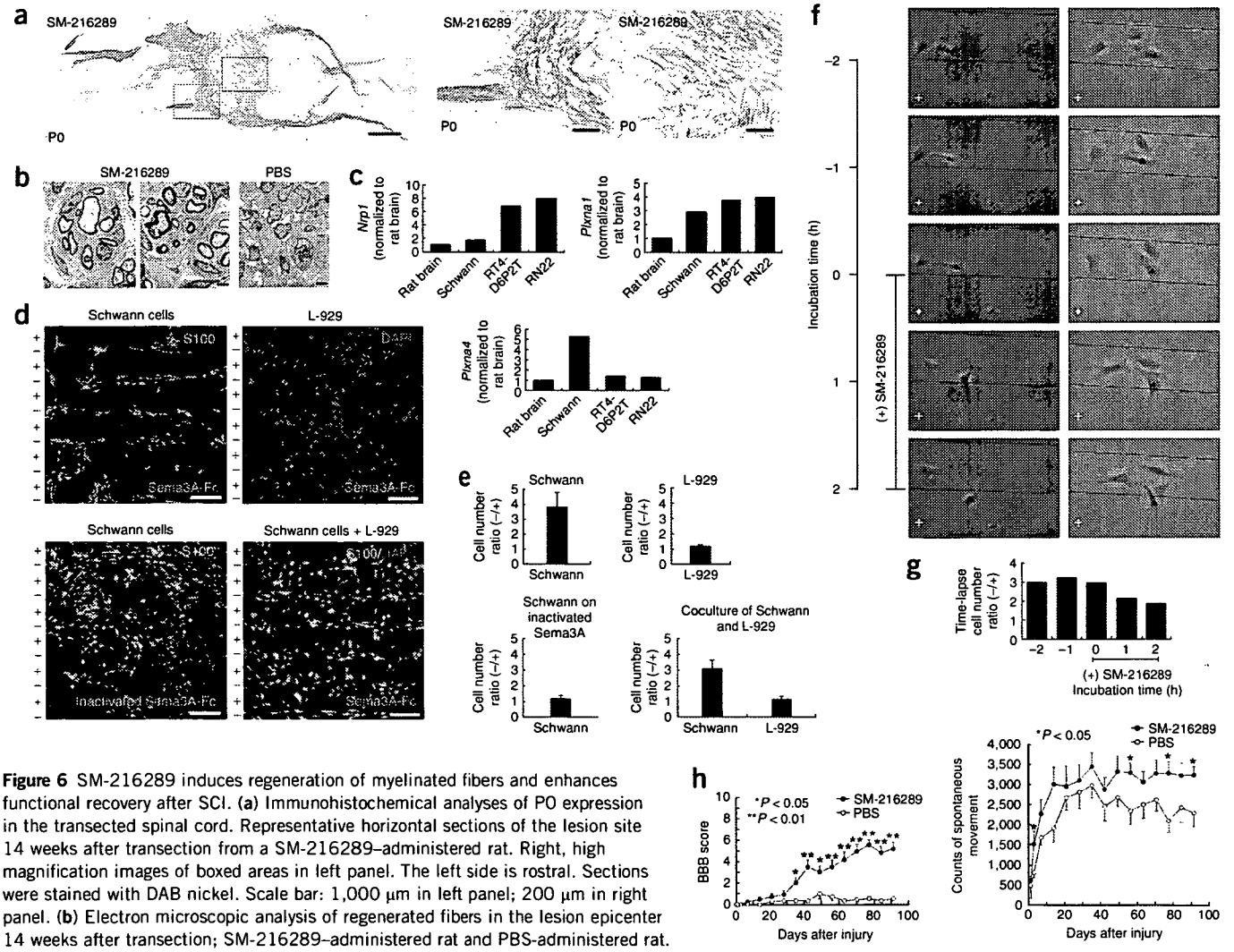

Figure 6 SM-216289 induces regeneration of myelinated fibers and enhances functional recovery after SCI. (**a**) Immunohistochemical analyses of P0 expression in the transected spinal cord. Representative horizontal sections of the lesion site 14 weeks after transection from a SM-216289–administered rat. Right, high magnification images of boxed areas in left panel. The left side is rostral. Sections were stained with DAB nickel. Scale bar: 1,000 μm in left panel; 200 μm in right panel. (**b**) Electron microscopic analysis of regenerated fibers in the lesion epicenter 14 weeks after transection; SM-216289–administered rat and PBS-administered rat. Representative transverse sections of the lesion epicenter. Scale bars, 2 μm. (**c**) Expression of Sema3A receptor components in Schwann cells. Total RNA was prepared from rat brain, primary Schwann cells and two Schwann cell–derived cell lines, and mRNA expression of *Nrp1*, *Plxna1* and *Plxna4* were analyzed with quantitative RT-PCR. Data normalized to expression level of rat brain are shown. (**d**) Schwann cells migration stripe assay. Schwann cells avoided stripes of immobilized Sema3A. Top left, Schwann cells were cultured on stripes of Sema3A-Fc and visualized in green by antibody to S100 (anti-S100; green). Top right, cells of the fibroblast cell line L-929, which do not express NP-1, were cultured on stripes of Sema3A-Fc and visualized by nuclei staining with 4′,6-diamidino-2-phenylindole (DAPI; blue). Bottom left, Sema3A-Fc was heat inactivated (65 °C, 30 min) before coating. Bottom right, a mixture of Schwann and L-929 cells was cultured on stripes of Sema3A-Fc and double-stained with anti-S100 (green) and DAPI (blue). Schwann cells were stained with anti-S100 (green, with blue nuclei); in contrast, L-929 cells were visualized only by their blue nuclei. Scale bars, 200 μm. (**e**) Ratio of the cell density between areas coated and noncoated with Sema3A-Fc. Bottom right, ratio of the cell density determined for Schwann cells and L-929 cells independently. Data represent mean ± s.d. (**f**) SM-216289 attenuates the Sema3A avoidance exhibited by Schwann cells. After preincubation (16 h), Schwann cells were incubated for 2 h before ($T = -2$ h to 0 h) and after ($T = 0$ h to 2 h) addition of SM-216289 (to be 200 μM as final concentration). Time-lapse photographs taken every hour (−2 h to 2 h) (two representative cell samples—one sample in each column—at each time point; arrowheads within a column indicate one particular cell within the sample). $T = 0$, time point at which SM-216289 was added to the culture. +, Sema3A-coated areas. Lines, boundaries of Sema3A-coated areas. (**g**) Relative cell densities (cell number ratio) at indicated time points in the time-lapse analysis. (**h**) Temporal functional analysis using BBB scoring (left) and temporal analysis of spontaneous movement using SCANET (right) up to 14 weeks after transection. Statistical analysis was performed using the Mann-Whitney *U*-test. Data are mean ± s.e.m.

abundantly in the lesion site in the SM-216289–administered group (**Fig. 6a**). We also confirmed the robust expression of *Nrp1*, *Plxna1* and *Plxna4* mRNA in Schwann cells using quantitative RT-PCR (**Fig. 6c**), suggesting that Schwann cells have the ability to respond to Sema3A or SM-216289. Also, using Sema3A-Fc fusion stripe assays, we found that Sema3A had a substantial repulsive effect on Schwann cell migration (**Fig. 6d,e**). When Schwann cells were cultured on the Sema3A stripe (made on a poly-L-ornithine substrate), Schwann cells avoided Sema3A-coated areas and preferentially distributed upon Sema3A-noncoated areas (**Fig. 6d,e**). The ratio of cell density between Sema3A-noncoated and Sema3A-coated areas ($Sema3A^-/Sema3A^+$) was 3.78 ± 0.98 (mean ± s.d.) in this experimental condition. To assess whether the behavior of Schwann cells depends on Sema3A signaling, we also examined the behavior of a Sema3A-insensitive fibroblast cell line, L-929, which does not express *Nrp1* mRNA (**Supplementary Fig. 4** online), on the same stripe as a negative control (in a pilot experiment, we confirmed using quantitative RT-PCR that the L-929 cells do not express *Nrp1* mRNA, although they do express *Plxna1* and *Plxna4* mRNA (**Supplementary Fig. 4**); therefore, they cannot respond to Sema3A). L-929 cells were randomly distributed on both Sema3A-coated and Sema3A-noncoated areas ($Sema3A^-/Sema3A^+$ = 1.17 ± 0.15). We also did not observe the avoiding behavior of Schwann cells on heat-inactivated Sema3A-Fc ($Sema3A^-/Sema3A^+$ = 1.18 ± 0.19; **Fig. 6d,e**). To confirm cell type–specific behavior on Sema3A stripes more directly, we cultured both Schwann cells and L-929 cells on these stripes. Schwann cells, but not L-929 cells, did not remain on Sema3A ($Sema3A^-/Sema3A^+$ = 3.05 ± 0.53 in Schwann, 1.19 ± 0.08 in L-929; **Fig. 6d,e**). These results clearly show that Schwann cells are sensitive to Sema3A and are repelled by Sema3A-coated areas. To examine more dynamically whether SM-216289 attenuates the repulsive effect of Sema3A against Schwann cells, we performed a time-lapse video analysis. Schwann cells were cultured on a Sema3A stripe for 16 h, and, using time-lapse video microscopy, we recorded the cell distribution on the stripe for 2 h before and after SM 216289 treatment. The population of cells that remained on Sema3A-noncoated areas markedly decreased even 1 h after SM-216289 treatment (**Fig. 6f,g**). This result suggests that inhibition of Sema3A can rapidly trigger Schwann cell migration into Sema3A-coated areas.

Presumably, the presence of peripheral-type myelin, which does not contain axonal growth inhibitors such as Nogo-A and OMgp (refs. 1–3,5,6), may contribute to the enhanced axonal regeneration observed. Our findings indicate that SM-216289 administration downregulates Sema3A signaling, upregulates regeneration-associated proteins in injured neurons and promotes Schwann cell–mediated myelination and axonal regeneration in the lesion site (**Figs. 4,5,6a–g**).

SM-216289 inhibits apoptosis and enhances angiogenesis

We found that SM-216289 also has a neuroprotective effect on cells at the lesion site after spinal cord transection injury (**Supplementary Note** and **Supplementary Fig. 5** online).

We also found enhanced angiogenesis at the lesion site in the SM-216289–administered rats (**Supplementary Note** and **Supplementary Fig. 5**).

SM-216289 promotes functional recovery after SCI

To examine the effect of SM-216289 on the rats' behavioral functions, we used the 21-point open-field Basso-Beattie-Bresnahan (BBB) locomotor rating scale (BBB scoring) to assess hindlimb movement[41] and the automated animal movement analysis system (SCANET) to measure spontaneous movement[42] of the rats. Hindlimb movement was significantly enhanced by the administration of SM-216289 (**Fig. 6h**; $P < 0.05$ at 5 and 7 weeks after injury; $P < 0.01$ at 6, 8, 9, 10, 11, 12 and 13 weeks after injury). In all the rats used in this study, hindlimb movement was abolished immediately after transection. Whereas hindlimb paralysis showed virtually no recovery in control rats (average BBB score: 0.55 ± 0.21 (mean ± s.e.m.) at 14 weeks after injury), hindlimb movement improved significantly in SM-216289–administered rats from 5 to 14 weeks after transection injury (average BBB score: 5.13 ± 0.57 at 14 weeks after injury). We also confirmed that the functional recovery resulted from the regeneration of axons in the lesion site rather than from recovery of autonomous function in the spinal cord below the lesion. For this purpose, the lesion site was retransected 10 weeks after the first transection, which resulted in a loss of recovered behavioral function (**Supplementary Fig. 6** online). The retransected rats' BBB scores dropped to 0 and remained at or below 1 for at least 5 weeks ($n = 5$). These retransection experiments suggested that the significant functional recovery observed in the treatment group was most probably caused by regeneration across the lesion site and not by compensatory response below the lesion site. Furthermore, we also found that by disrupting the serotonergic (5-HT–positive) raphespinal tract using the serotonin neurotoxin 5,7-dihydroxytryptamine (DHT) as previously described[11], the functional recovery observed in the SM-216289–administered group ($P < 0.05$ at 4, 9 and 10 weeks after injury; $P < 0.01$ at 6, 7 and 8 weeks after injury) could be substantially attenuated (**Supplementary Fig. 6**). This suggested that the enhanced regeneration of serotonergic (5-HT–positive) raphespinal tract was at least partly responsible for the improved functional recovery observed in the SM-216289–administered group.

Spontaneous movement was also significantly enhanced in the SM-216289–administered rats when compared with control rats ($P < 0.05$ at 3 d and 8, 11 and 13 weeks after injury; **Fig. 6h**). However, at some early time point, we observed a significant difference in spontaneous movement that was not reflected in BBB scores (**Fig. 6h**), indicating that the observed early effects of SM-216289 may have resulted from mechanisms other than axonal regeneration across the lesion site—for instance, local neuroprotective effects.

DISCUSSION

The current study has two major findings: first, that Sema3A contributes considerably to the inadequate axonal regeneration at the spinal cord lesion site after transection injury; and second, that SM-216289 strongly inhibits the Sema3A signal both *in vivo* and *in vitro*, and is an effective promoter of regenerative responses including axonal regeneration and/or preservation, Schwann cell–mediated myelination and axonal regeneration, angiogenesis, and the inhibition of apoptosis after spinal cord transection.

The involvement of Sema3A in an *in vivo* experimental animal model of SCI has been described in several reports[13,14,16]. For instance, a previous study showed using *in situ* hybridization that *Sema3a* mRNA expression is upregulated within the fibronectin-positive scar tissue following transection and contusion injuries in the adult rat spinal cord. The same study also showed that two major descending spinal cord motor pathways, the corticospinal and rubrospinal tracts, continue to express mRNA of receptor components for Sema3A after injury, suggesting that these axon tracts may be potentially sensitive to Sema3A within the scar tissue. Consistently, most descending fibers did not penetrate the *Sema3a* mRNA–expressing portion of the scar tissue at the lesion site[16]. These results suggest that Sema3A contributes to the inhibitory properties of the scar tissue, thereby inhibiting successful regeneration of injured axons.

These findings, however, do not provide direct evidence that Sema3A contributes significantly to the inhibitory properties of the lesion site in the spinal cord after injury. But as mentioned earlier, because the high lethality of *Sema3a*$^{-/-}$ mice precludes an adequate genetic assessment of the contribution of Sema3A to the limited regeneration of the injured spinal cord, we decided to use a pharmacological approach as an alternative method. In this study, neutralizing Sema3A created a permissive environment for the regeneration of injured spinal cord axons. Our findings thus indicate more directly that Sema3A contributes substantially to the inhibitory properties of the lesion site in the spinal cord after transection. However, we also observed that in SM-216289–administered rats, there was no axonal regeneration of long axon tracts other than 5-HT–positive raphespinal tract axons (which include CST and ascending dorsal column fibers), consistent with the results from *Sema3a*$^{-/-}$ mice. Our data thus indicate that the contribution of Sema3A to regenerative incompetency is considerable but limited.

There are several possible explanations for the markedly enhanced functional recovery observed in SM-216289–administered rats. Although we detected the enhanced regeneration and/or preservation of axons in the lesion site, we did not observe that axons in some long axon tracts such as the CST penetrated the lesion site (**Figs. 4** and **5**). However, past studies using complete transection injury models have rarely provided convincing evidence of corticospinal tract regeneration, most probably due to the existence of a gap of a few millimeters between the severed ends of the spinal cord (which results in enormous scar tissue area) in the lesion site after transection injury. Notably, although we did not observe extensive serotonergic raphespinal tract axons[11,36] in the spinal cord at locations far caudal to the lesion site in either group, we did identify considerably more 5-HT–positive axons within and across the lesion site (**Fig. 5b–d**) in the SM-216289–administered group. Furthermore, we also found that by disrupting the serotonergic raphespinal tract using 5,7-DHT as previously described[11], the functional recovery observed in the SM-216289–administered group could be markedly attenuated, which suggests that a considerably enhanced regeneration of raphespinal tract fibers may be at least partly responsible for the improved functional recovery observed in this group. It has been reported that disrupting Nogo receptor signaling using genetic approaches could promote the regeneration of serotonergic raphespinal tract axons across the lesion site into the side far caudal to the lesion site[11]. Therefore, it is possible that in order to obtain further regeneration of serotonergic fibers in the raphespinal tract, inhibitory signals other than Sema3A may also need to be disrupted.

It is also plausible that the regenerated axons observed in the lesion site of SM-216289–administered rats may include preserved and regenerated short projection neurons or interneurons. The increased number of axons in the lesion site in the SM-216289–administered group may have arisen from enhanced neuroprotection, which protects axons from retraction or degeneration and gives them a higher probability of regeneration. A recent study reported that regenerating local axons, consisting mainly of interneurons, can form intraspinal neural circuits in the lesion site after spinal cord injury and make synaptic connections with CST collaterals[43]. Although this study used a hemisection model, which is different from our current model, it is plausible that this kind of mechanism, with signal relay via short regenerated neuronal fibers, may also be responsible for the functional recovery[43]. In addition, our retransection experiments suggest that the functional recovery observed in the treatment group is most probably caused by regeneration within and across the lesion site, and not by compensatory responses below the lesion site.

A second possible mechanism involves the enhancement of Schwann cell migration by SM-216289 administration, along with a guidance role for Schwann cells in axonal regeneration and in the promotion of myelination of the regenerated fibers. Sema3A has been reported to be involved in some forms of cell migration[37–39]. In SM-216289–administered rats, most of the regenerated axons were myelinated by Schwann cells, an observation rarely made in control rats (**Fig. 6b**). These findings indicate that Schwann cells had extensively migrated into the lesion site in SM-216289–administered rats, that they had guidance roles in axonal regeneration and that they contributed to the myelination of regenerated fibers. In support of this hypothesis, we confirmed the robust expression of *Nrp1*, *Plxna1* and *Plxna4* mRNA in Schwann cells (by quantitative RT-PCR) (**Fig. 6c**). Using an *in vitro* stripe assay, we also found that Sema3A repels Schwann cells (**Fig. 6d,e**) and, furthermore, that SM-216289 attenuates this repulsive response (**Fig. 6f,g**). These results support the hypothesis that Schwann cell migration into the lesion site may be affected by Sema3A activity. Also, considering a previous report describing the effect of Sema3A on neural crest cell migration[37], it is also possible that immature neural crest–derived cells putatively present in the peripheral nerve[44] can migrate into the lesion site within the injured spinal cord, where they may then mature into Schwann cells. This peripheral-type myelination, which does not involve axonal growth inhibitors such as Nogo-A and OMgp, is considered to be favorable for axonal regeneration and may play a guidance role in axonal regeneration.

Two other potential mechanisms are discussed in the **Supplementary Discussion** online. We consider these and the two possibilities discussed above to be the major mechanisms that may be responsible for the functional recovery observed in this study.

As mentioned earlier, studies using Nogo[8–10] and Nogo receptor knockout mice[11,12], as well as other reports[13–16], support the idea that axonal growth inhibitors other than myelin-associated proteins are present, and that these must be overcome for adequate axonal regeneration to occur. Among them, extracellular matrix molecules have been regarded as key molecules limiting axonal regeneration after SCI.

In this study, we targeted Sema3A (refs. 13,14,16,19–24), which, in addition to CSPGs (refs. 15,17,18), has been reported to be a major extracellular matrix molecule inhibiting axonal regeneration. We consequently demonstrated that SM-216289 (refs. 25,26) can strongly and selectively inhibit Sema3A signaling both *in vitro* and *in vivo*, and, most importantly, provided evidence that this compound is a potentially effective agent for promoting axonal regeneration after spinal cord transection.

To achieve further axonal regrowth, including the regeneration of long fiber tracts, the concomitant use of SM-216289 with other therapeutic modalities such as neurotrophic factors[45], soluble Nogo receptors[7], chondroitinase ABC (ref. 15), or tissue or cell transplantation[36], could potentially be beneficial. As a model for SCI, the transection protocol is appropriate for assessing axonal regeneration, but it does not fully parallel SCI in the clinical setting. In contrast, the contusion model may be more representative of human SCI because it reveals features similar to those seen in the clinical context. Therefore, future studies should focus on the concurrent use of SM-216289 with other treatments, its application to contusion lesions, or its application to nonhuman primates. In conclusion, this study demonstrates that Sema3A plays an essential role in regenerative failure (including the inhibition of axonal regeneration) after SCI and that SM-216289 may be a possible therapeutic agent for human SCI.

METHODS

Animals and surgical procedures. We used adult female Sprague-Dawley rats weighing 200–250 g in this study. All aspects of animal care and treatment were carried out according to the guidelines of the experimental animal care committee of Keio University, School of Medicine. Anesthetized (sodium pentobarbital, 40 mg per kg body weight) rats received complete spinal cord transections at the Th8 lamina level using procedures described previously[36]. Briefly, after Th8 laminectomy, the dura was opened, and the spinal cord was transected using a surgical blade (Feather). The severed ends of the cord typically retracted about 3 mm and were inspected under a surgical microscope to ensure complete transection. The muscles and skin were closed in layers. The administration of SM-216289 is described in detail in a later section. After the operation, the rats were kept warm, placed on beds of sawdust, and given manual bladder evacuation twice per day and intramuscular injection of ampicillin (50 mg once per day up to 1 week after transection) to prevent infections. To prevent dehydration, rats were hydrated with up to 20 ml per day of lactated Ringer's solution or normal saline injected intraperitoneally (i.p.). Food was provided on the cage floor, and the rats had no difficulty reaching their water bottles. Supplemental oral feedings were given as necessary. Surgeries for retransection were performed 10 weeks after the first transection in the same manner ($n = 5$).

For axon tract tracing, rats received six stereotaxic injections of 10% biotinylated dextran amine (BDA, Molecular Probes) in the sensorimotor cortex of the bilateral forelimb and hindlimb region ($n = 6$) 8 weeks after the transection injury. For each injection, 0.5 μl BDA was delivered over a period of 2 min by means of a glass pipette (inner diameter 10–15 μm) attached to a nanoinjector (Stoelting). These BDA-injected rats were killed 14 d after the injection. Nine weeks after transection, cholera toxin B subunit (CTB, 1%, List Biological Lab) was injected into the sciatic nerves bilaterally ($n = 4$). For each injection, 5 μl CTB was delivered over a period of 20 s by means of a glass pipette (inner diameter 10–15 μm) attached to the nanoinjector (Stoelting). These CTB-injected rats were killed 5 d after the injection.

For the rats receiving bilateral intracerebroventricular (i.c.v.) injections of the serotonin neurotoxin DHT (300 μg dissolved in 5 μl of 0.2% ascorbic acid in normal saline), the procedure was performed as described[11] with slight modification 10 weeks after complete transection ($n = 8$: 4 each in the SM-216289 and PBS groups). Thirty minutes before the 5,7-DHT injection, we administered the monoamine uptake inhibitor desipramine (25 mg/kg, i.p.; Sigma).

In this study, we also used *Sema3a*-deficient mice as described in a previous report[22]. We obtained *Sema3a*$^{-/-}$ homozygous mutant mice through *in vitro* fertilization and applied almost identical surgical procedures as described above for rats to the *Sema3a*$^{-/-}$ mice and control wild-type C57/BL6 mice, using smaller dosages of tracers.

See **Supplementary Methods** online for details of the primary antibodies used; the immunohistochemistry, *in situ* hybridization and immunoblotting procedures; the preparation of SM-216289 by fermentation of the *Penicillium* sp. strain SPF-3059; the pharmacological profiling of SM-216289; and the cell growth assay.

Quantification for immunohistochemistry. Quantification of each marker's immunoreactive density was performed using the MCID Elite System (Imaging Research Inc.) as described[46] with slight modifications[47,48]. Details are available in the **Supplementary Methods**.

Growth cone collapse assay. The growth cone collapse assay was performed as described in ref. 20 with slight modifications[23,25]. Details are available in the **Supplementary Methods**.

Co-culture assay in collagen gel. Collagen co-culture experiments were performed as described previously[49] with slight modifications[25]. Details are available in **Supplementary Methods**.

Administration of SM-216289 into the injured spinal cord. At the time of transection injury, we placed an osmotic mini-pump (Alzet) underneath the back skin and guided the attached tube into the lesion site. We performed this tubing procedure so that the exit from the osmotic mini-pump's tube was set just above the lesion epicenter, thus ensuring that SM-216289 had direct access to the lesion. We administered SM-216289 (0.1 mg/ml, 0.174 mM) through the osmotic mini-pump for 4 weeks (0.25 μl/h, 0.6 μg/d) after the injury. For the control rats, we delivered the same amount of PBS instead of SM-216289.

After the administration of SM-216289 into the injured spinal cord, we conducted an immunoblotting analysis of the molecules downstream of Sema3A, and also analyzed the apoptotic cells. Details of both procedures are in **Supplementary Methods**, along with information pertaining to the electron microscopic analysis, quantitative RT-PCR and behavioral analysis.

Schwann cell migration stripe assay. Schwann cells were prepared from sciatic nerves of P7 Wistar rats as described[50] with slight modifications. Details are available in the **Supplementary Methods**.

Note: Supplementary information is available on the Nature Medicine website.

ACKNOWLEDGMENTS

We are grateful to L. Benowitz (Children's Hospital Boston); H. Fujisawa (Nagoya University); A.L. Kolodkin (Johns Hopkins University); and Y. Ihara and K. Mori (Tokyo University) for reagents. We also thank M. Dezawa, S. Kawabata, U. Uchida, Y. Sugiyama, F. Nakamura, T. Nagai, S. Miyao, T. Harada, K. Watanabe, H. Hanafusa, Y. Ujimasa, T. Yagi and G. Yiu for technical assistance. We are also grateful to T. Takahashi, H. Fujisawa and F. Murakami for their critical reading of the manuscript, to the members of the Okano Laboratory for their comments on the manuscript. This work was supported by grants from the Leading Project for Realization of Regenerative Medicine from the Ministry of Education, Culture, Sports, Science and Technology (MEXT), Japan; the Japan Science and Technology Corporation (JST); and the General Insurance Association of Japan. This work was also supported by a Keio University special grant-in-aid for innovative collaborative research projects to H.O.; a Keio University grant-in-aid for encouragement of young medical scientists to S.K. and A.I.; and a grant-in-aid from the 21st Century COE Program of MEXT, Japan, to Keio University.

AUTHOR CONTRIBUTIONS

S.K. wrote the manuscript, conducted all the SCI experiments (including preparation of the SCI model rats, and behavioral and histochemical characterizations), conducted *in vitro* assays (including growth cone collapse assay) and all the immunoblotting, and prepared the recombinant proteins. A.I. conducted rat SCI experiments as detailed above, conducted SCI experiments of *Sema3a*-deficient mice, and cowrote the manuscript. M.N. instructed S.K. and A.I. on the technical aspects of the SCI experiments, and cowrote the manuscript. A.K. conducted histochemical characterization of SCI model rats. K. Kikuchi conducted *in vitro* experiments (including collagen gel coculture, KB-cell cell growth assay and Schwann cell migration assay). S.S. conducted cell preparation for the *in vitro* migration assay. H.J.O. prepared the recombinant proteins. T.I. participated in SCI experiments including behavioral characterizations. A.M. prepared the recombinant semaphorin proteins. O.K participated in histochemical characterization of SCI model rats. C.N. organized the collaboration with Keio University at Dainippon Sumitomo. K. Kumagai prepared SM-216289 and examined its specificity of action *in vitro*. T.K. supervised the SM-216289 project at Dainippon Sumitomo. Y.S. and Y.G. examined the specificity of SM-216289's effect on Sema3A by growth cone collapse assay. M.T. provided and conducted the genetic diagnosis of *Sema3a*-deficient mice. M.I. conducted the *in vitro* fertilization of *Sema3a*-deficient mice. Z.H. provided advice on the experimental design. Y.T. supported and supervised the SCI experiments conducted at Keio University. H.O. supervised the whole project and cowrote the manuscript with S.K., A.I. and M.N.

COMPETING INTERESTS STATEMENT

The authors declare that they have no competing financial interests.

Published online at http://www.nature.com/naturemedicine
Reprints and permissions information is available online at http://npg.nature.com/reprintsandpermissions/

1. Schwab, M.E., Kapfhammer, J.P. & Bandtlow, C.E. Inhibitors of neurite growth. *Annu. Rev. Neurosci.* **16**, 565–595 (1993).
2. GrandPre, T., Nakamura, F., Vartanian, T. & Strittmatter, S.M. Identification of the Nogo inhibitor of axon regeneration as a reticulon protein. *Nature* **403**, 439–444 (2000).
3. Chen, M.S. *et al.* Nogo-A is a myelin-associated neurite outgrowth inhibitor and an antigen for monoclonal antibody IN-1. *Nature* **403**, 434–439 (2000).

4. Domeniconi, M. *et al.* Myelin-associated glycoprotein interacts with the Nogo66 receptor to inhibit neurite outgrowth. *Neuron* **35**, 283–290 (2002).
5. Olson, L. Medicine: clearing a path for nerve growth. *Nature* **416**, 589–590 (2002).
6. Wang, K.C. *et al.* Oligodendrocyte-myelin glycoprotein is a Nogo receptor ligand that inhibits neurite outgrowth. *Nature* **417**, 941–944 (2002).
7. Li, S. *et al.* Blockade of Nogo-66, myelin-associated glycoprotein, and oligodendrocyte myelin glycoprotein by soluble Nogo-66 receptor promotes axonal sprouting and recovery after spinal injury. *J. Neurosci.* **24**, 10511–10520 (2004).
8. Kim, J.E., Li, S., GrandPre, T., Qiu, D. & Strittmatter, S.M. Axon regeneration in young adult mice lacking Nogo-A/B. *Neuron* **38**, 187–199 (2003).
9. Simonen, M. *et al.* Systemic deletion of the myelin-associated outgrowth inhibitor Nogo-A improves regenerative and plastic responses after spinal cord injury. *Neuron* **38**, 201–211 (2003).
10. Zheng, B. *et al.* Lack of enhanced spinal regeneration in Nogo-deficient mice. *Neuron* **38**, 213–224 (2003).
11. Kim, J.E., Liu, B.P., Park, J.H. & Strittmatter, S.M. Nogo-66 receptor prevents raphespinal and rubrospinal axon regeneration and limits functional recovery from spinal cord injury. *Neuron* **44**, 439–451 (2004).
12. Zheng, B. *et al.* Genetic deletion of the Nogo receptor does not reduce neurite inhibition *in vitro* or promote corticospinal tract regeneration *in vivo*. *Proc. Natl. Acad. Sci. USA* **102**, 1205–1210 (2005).
13. Pasterkamp, R.J. *et al.* Expression of the gene encoding the chemorepellent semaphorin III is induced in the fibroblast component of neural scar tissue formed following injuries of adult but not neonatal CNS. *Mol. Cell. Neurosci.* **13**, 143–166 (1999).
14. Pasterkamp, R.J., Anderson, P.N. & Verhaagen, J. Peripheral nerve injury fails to induce growth of lesioned ascending column axons into spinal cord scar tissue expressing the axon repellent Semaphorin3A. *Eur. J. Neurosci.* **13**, 457–471 (2001).
15. Bradbury, E.J. *et al.* Chondroitinase ABC promotes functional recovery after spinal cord injury. *Nature* **416**, 636–640 (2002).
16. De Winter, F. *et al.* Injury-induced class 3 semaphorin expression in the rat spinal cord. *Exp. Neurol.* **175**, 61–75 (2002).
17. Morgenstern, D.A., Asher, R.A. & Fawcett, J.W. Chondroitin sulphate proteoglycans in the CNS injury response. *Prog. Brain Res.* **137**, 313–332 (2002).
18. Silver, J. & Miller, J.H. Regeneration beyond the glial scar. *Nat. Rev. Neurosci.* **5**, 146–156 (2004).
19. Kolodkin, A.L., Matthes, D.J. & Goodman, C.S. The semaphorin genes encode a family of transmembrane and secreted growth cone guidance molecules. *Cell* **75**, 1389–1399 (1993).
20. Luo, Y., Raible, D. & Raper, J.A. Collapsin: a protein in brain that induces the collapse and paralysis of neuronal growth cones. *Cell* **75**, 217–227 (1993).
21. Goshima, Y., Nakamura, F., Strittmatter, P. & Strittmatter, S.M. Collapsin-induced growth cone collapse mediated by an intracellular protein related to *unc-33*. *Nature* **376**, 509–514 (1995).
22. Taniguchi, M. *et al.* Disruption of semaphorin III/D gene causes severe abnormality in peripheral nerve projection. *Neuron* **19**, 519–530 (1997).
23. Sasaki, Y. *et al.* Fyn and Cdk5 mediate semaphorin-3A signaling which is involved in regulation of dendrite orientation in cerebral cortex. *Neuron* **35**, 907–920 (2002).
24. Uchida, Y. *et al.* Semaphorin-3A signaling is mediated via sequential Cdk5 and GSK3b phosphorylation of CRMP2: implication of common phosphorylating mechanism underlying axon guidance and Alzheimer's disease. *Genes Cells* **10**, 165–179 (2005).
25. Kikuchi, K. *et al. In vitro* and *in vivo* characterization of a novel Semaphorin 3A inhibitor, SM-216289 or xanthofulvin. *J. Biol. Chem.* **278**, 42985–42991 (2003).
26. Kumagai, K., Hosotani, N., Kikuchi, K., Kimura, T. & Saji, I. Xanthofulvin, a novel semaphorin inhibitor produced by a strain of *Penicillium*. *J. Antibiot.* **56**, 610–616 (2003).
27. He, Z. & Tessier-Lavigne, M. Neuropilin is a receptor for the axonal chemorepellent semaphorin III. *Cell* **90**, 739–751 (1997).
28. Kitsukawa, T. *et al.* Neuropilin-semaphorin III/D-mediated chemorepulsive signals play a crucial role in peripheral nerve projection in mice. *Neuron* **19**, 995–1005 (1997).
29. Kolodkin, A.L. *et al.* Neuropilin is a Semaphorin III receptor. *Cell* **90**, 753–762 (1997).
30. Takahashi, T. *et al.* Plexin-neuropilin-1 complexes form functional semaphorin-3A receptors. *Cell* **99**, 59–69 (1999).
31. Tamagnone, L. *et al.* Plexins are a large family of receptors for transmembrane, secreted, and GPI-anchored semaphorins in vertebrates. *Cell* **99**, 71–80 (1999).
32. Yaron, A., Huang, P.H., Cheng, H.J. & Tessier-Lavigne, M. Differential requirement for Plexin-A3 and -A4 in mediating responses of sensory and sympathetic neurons to distinct class 3 Semaphorins. *Neuron* **45**, 513–523 (2005).
33. Christensen, M.D. & Hulsebosch, C.E. Spinal cord injury and anti-NGF treatment results in changes in CGRP density and distribution in the dorsal horn in the rat. *Exp. Neurol.* **147**, 463–475 (1997).
34. Romero, M.I. *et al.* Extensive sprouting of sensory afferents and hyperalgesia induced by conditional expression of nerve growth factor in the adult spinal cord. *J. Neurosci.* **20**, 4435–4445 (2000).
35. Romero, M.I., Rangappa, N., Garry, M.G. & Smith, G.M. Functional regeneration of chronically injured sensory afferents into adult spinal cord after neurotrophin gene therapy. *J. Neurosci.* **21**, 8408–8416 (2001).
36. Bregman, B.S. Spinal cord transplants permit the growth of serotonergic axons across the site of neonatal spinal cord transection. *Brain Res.* **431**, 265–279 (1987).
37. Eickholt, B.J., Mackenzie, S.L., Graham, A., Walsh, F.S. & Doherty, P. Evidence for collapsin-1 functioning in the control of neural crest migration in both trunk and hindbrain regions. *Development* **126**, 2181–2189 (1999).
38. Bagnard, D. *et al.* Semaphorin 3A-vascular endothelial growth factor-165 balance mediates migration and apoptosis of neural progenitor cells by the recruitment of shared receptor. *J. Neurosci.* **21**, 3332–3341 (2001).
39. Bagri, A. & Tessier-Lavigne, M. Neuropilins as Semaphorin receptors: *in vivo* functions in neuronal cell migration and axon guidance. *Adv. Exp. Med. Biol.* **515**, 13–31 (2002).
40. Archelos, J.J. *et al.* Production and characterization of monoclonal antibodies to the extracellular domain of P0. *J. Neurosci. Res.* **35**, 46–53 (1993).
41. Basso, D.M., Beattie, M.S. & Bresnahan, J.C. A sensitive and reliable locomotor rating scale for open field testing in rats. *J. Neurotrauma* **12**, 1–21 (1995).
42. Mikami, Y. *et al.* A simple and reliable behavioral analysis of locomotor function after spinal cord injury in mice. Technical note. *J. Neurosurg.* **97**, 142–147 (2002).
43. Bareyre, F.M. *et al.* The injured spinal cord spontaneously forms a new intraspinal circuit in adult rats. *Nat. Neurosci.* **7**, 269–277 (2004).
44. Morrison, S.J., White, P.M., Zock, C. & Anderson, D.J. Prospective identification, isolation by flow cytometry, and *in vivo* self-renewal of multipotent mammalian neural crest stem cells. *Cell* **96**, 737–749 (1999).
45. Cai, D., Shen, Y., De Bellard, M., Tang, S. & Filbin, M.T. Prior exposure to neurotrophins blocks inhibition of axonal regeneration by MAG and myelin via a cAMP-dependent mechanism. *Neuron* **22**, 89–101 (1999).
46. McTigue, D.M., Horner, P.J., Stokes, B.T. & Gage, F.H. Neurotrophin-3 and brain-derived neurotrophic factor induce oligodendrocyte proliferation and myelination of regenerating axons in the contused adult rat spinal cord. *J. Neurosci.* **18**, 5354–5365 (1998).
47. Ikegami, T. *et al.* Chondroitinase ABC combined with neural stem/progenitor cell transplantation enhances graft cell migration and outgrowth of growth-associated protein-43-positive fibers after rat spinal cord injury. *Eur. J. Neurosci.* **22**, 3036–3046 (2005).
48. Okada, S. *et al.* Conditional ablation of Stat3 or Socs3 discloses a dual role for reactive astrocytes after spinal cord injury. *Nat. Med.* **12**, 829–834 (2006).
49. Guthrie, S. & Lumsden, A. Collagen gel coculture of neural tissue. *Neuroprotocols* **4**, 116–120 (1994).
50. Thomaidou, D. *et al.* Soluble forms of NCAM and F3 neuronal cell adhesion molecules promote Schwann cell migration: identification of protein tyrosine phosphatases zeta/beta as the putative F3 receptors on Schwann cells. *J. Neurochem.* **78**, 767–778 (2001).

3. 筋萎縮性側索硬化症のAMPA受容体仮説

東京大学大学院医学系研究科脳神経医学専攻神経内科学　日出山拓人
同　神経内科学准教授　郭　　伸

key words　ALS, AMPA receptor, GluR2, ADAR2, RNA editing

要　旨

我々のグループは，孤発性ALS脊髄運動ニューロンでは，グルタミン酸受容体であるAMPA（α-3-hydroxy-5-methyl-4-isoxazole propionic acid）受容体サブユニットの一つであるGluR2のQ/R部位にRNA編集が起こらない未編集型のGluR2増加が，疾患特異的，細胞選択的に起こっていることを見いだし，この分子変化がチャネルのCa^{2+}透過性亢進を通じて神経細胞死の直接原因になり，しかも変異SOD1関連家族性ALSを含めた他の神経変性疾患にはみられないことから，孤発性ALSの病因と考えられることを明らかにした[1]．私たちのグループの仮説の詳細は別稿を参照されたい[2,3]．本稿では，ALSのAMPA受容体仮説に至るまでの歴史的な経緯と背景を紹介する．機能分子の異常が細胞死と直結している点でこの仮説を証明することが，病因の解明のみならず特異的治療への道を切りひらく可能性があると考えている．

動　向

ALSは，1870年代にJean-Martin Charcotにより疾患概念が確立してから約140年となるが，今なお原因不明で運動ニューロンだけがある時期からなぜ突然死ぬのか，という機序は依然として解明されていない．孤発性ALSは全患者の90%以上を占め，中毒説（農薬，鉛，水銀，アルミニウム，ALSと病態の似ている南アジアや東アフリカの地方病neurolathylismとの関連が疑われているエジプト豆に含有されるβ-N-oxalylamino-L-alanine: BOAA，グアム島のALS PD dementia complexの原因とされたソテツ中のアミノ酸β-N-methylamino-L-alanine: BMAAなど），神経栄養因子欠乏説，細胞骨格タンパク異常説，逆行性軸索流異常説（dynein/dynactin）などが検討されてきたが，いずれも証明されていない．最も有力な仮説は，グルタミン酸受容体サブタイプであるAMPA受容体を介した興奮性神経細胞死仮説であり，中でも我々が見いだした孤発性ALS運動ニューロン選択的に生じているAMPA受容体のGluRサブユニットmRNAのRNA編集異常は，高い疾患特異性をもち，かつ神経細胞死の一次原因であることから孤発性ALSの病因と密接に関連すると考えられ，これを支持する知見が積み重ねられ現在に至っている．

A. 興奮性神経細胞死とは？

錐体路はグルタミン酸が神経伝達物質であり，脊髄運動ニューロンもこの興奮性入力を豊富に受

けている．そのため運動ニューロンにおいてもグルタミン酸受容体が高密度で発現しており[4]，グルタミン酸による興奮が過剰になるとCa^{2+}などのイオン透過性亢進が引き起こされ，細胞内環境の変化を補償する機能を越えてしまい，その結果として細胞死のカスケードが働く，というのが興奮性神経細胞死のメカニズムである．これは，主に虚血や低血糖，外傷，てんかん重積などの急性の神経細胞死に働くと考えられていた[5]．一方で近年，培養細胞系，*in vivo*動物実験系で急性には神経細胞死を引き起こさない濃度でも受容体が長期間持続的に興奮することで遅発性の神経細胞死が起こることが次々と明らかにされ，特にALSでグルタミン酸受容体を介した経路が関与している可能性が注目されるようになった[6,7]．

動物実験では器官培養脊髄の前角運動ニューロンにおいて培養液中にグルタミン酸トランスポーターの阻害剤を加えると変性が起こり[8]，長期間持続的にトランスポーターをコードするmRNAのアンチセンスmRNAを投与し，トランスポータータンパクの発現を抑えるとラット脊髄運動ニューロンに変性が生じた．また，ラット脊髄クモ膜下腔にグルタミン酸トランスポーター阻害剤であるTHAを投与することにより，AMPA受容体を介した遅発性の神経細胞死が後角ニューロンに生ずる[9]．これらの結果から，グルタミン酸トランスポーターの異常によりシナプス間隙のグルタミン酸濃度が上昇すると脊髄運動ニューロンが障害されることが示された．この神経細胞死はAMPA受容体アンタゴニストにより回避されるのでAMPA受容体の持続的興奮が関与していることが示されている．さらに，プライマリーカルチャーでは，脊髄前角ニューロンは後角ニューロンに比べ，AMPA受容体アゴニストに対する毒性に脆弱であること[10]，AMPA受容体アゴニストを長時間持続的にラット脊髄クモ膜下腔に投与すると後角脊髄ニューロンに遅発性の神経細胞死を起こし[11]，特にカイニン酸の4～8週間の持続投与では運動ニューロンが選択的に変性することが*in vivo*実験で示され[12]，AMPA受容体の持続的興奮により運動ニューロンに遅発性の神経細胞死が起きることが様々な実験系で示された．これらはAMPA受容体を介する神経細胞死がALSの神経細胞死に働いていることを示唆するものである[2,3]．

B. 神経細胞死とAMPA受容体

グルタミン酸受容体は大きくイオンチャネル型と代謝調節型に分類される．そしてイオンチャネル型はさらにNMDA受容体，カイニン酸受容体，AMPA受容体に分けられる．NMDA受容体が急性の神経細胞死に関与するのに対して特に速いシナプス伝達にかかわるAMPA受容体は，ニューロンの遅発性の細胞死に関与し，運動ニューロンは，特に後者の興奮性細胞死に脆弱であることが知られている．その分子メカニズムとして細胞死に先立つ過剰なCa^{2+}流入による細胞内Ca^{2+}濃度の持続的上昇が培養ニューロンで明らかにされ，それに引き続くCa^{2+}依存性プロテアーゼの活性化，ミトコンドリア障害，NOS産生などによるカスケードが細胞死を引き起こすことが様々な実験系により明らかにされた[13]．神経細胞内Ca^{2+}濃度上昇の機構には，1）NMDA受容体の活性化によるチャネルからのCa^{2+}流入，2）Ca^{2+}透過性AMPA受容体の活性化，3）代謝型グルタミン酸受容体などの興奮によるIP3産生を介する小胞体からのCa^{2+}動員，4）膜の脱分極による膜電位依存性Ca^{2+}チャネルの開口などのメカニズムが知られている[14]．最近は電位非依存性カチオン透過性チャネルの関与も示唆されている（例：transient receptor potential，以下TRP）[15]．なぜ神経細胞死にAMPA受容体のCa^{2+}透過性の関与が大きいのか，についてはまだ不明な点が多い

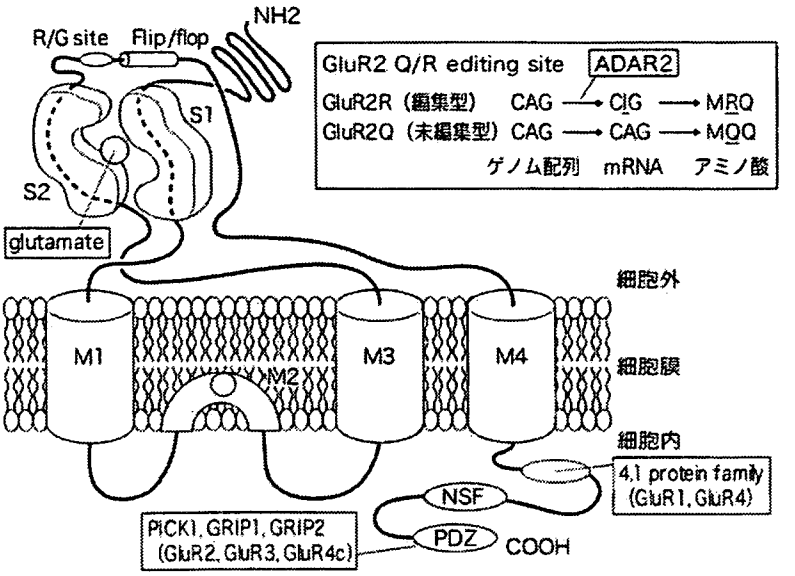

図1　AMPA受容体の構造（文献2,3,16-20より改変）

AMPA受容体は4種類のサブユニットGluR1～GluR4から構成される4量体からなる．M1～M4は膜ドメイン．S1とS2は仮想的グルタミン酸結合部位．各サブユニットにはそれぞれ選択的スプライシングにより異なるアミノ酸配列をもったflip型とflop型という2つのタイプがあり，発生時期や脳の部位で異なっている．GluR2～4にはR/G部位があり，RNA編集によりアルギニン（R）からグリシン（G）へ置換する．この部位は受容体脱感作を修飾する．さらにGluR2の多様性が生じるメカニズムとしてM2に存在するQ/R編集部位があり，翻訳過程でCAGまたはCAA（グルタミン（Q））がCGGまたはCGA（アルギニン（R））になる．そのため，サブユニットの組み合わせの違いが機能的な多様性をもたらすと推測される．細胞内C末端領域にはPKA，PKC，CaMKIIによるリン酸化部位やGRIP，PICK，SAP97などのPDZタンパク質結合部位が局在する．この領域はPDZドメインを介してGRIPなどpostsynaptic density（PSD）タンパクと結合し，シナプスでのAMPA受容体の安定化などにかかわっている．また，AMPA受容体はTARPタンパク（本文参照），stargazinタンパク（VDCC γ2），VDCC γ3-8と膜表面で共在することが知られており，これらのタンパクがチャネル活性とかかわっていることがわかっている．

PDZ: Postsynaptic density-95/Discs large/Zona occuludens-1,
PKA: protein kinase A, PKC: protein kinase A,
CaMKII: Ca^{2+}/ calmodulin-dependent protein kinase phosphates II, GRIP1: glutamate receptor-interacting protein type 1, GRIP2: glutamate receptor-interacting protein type 2,
PICK: protein that interacts with C kinase, SAP97: synapse-associated protein 97,
NSF: N-ethylmaleamide sensitive factor, PSD: postsynapitic density,
VDCC: voltage-dependent Ca^{2+} channel
図中のCIGは，リボソームでIはグアノシン（G）と同等であると見なされるため，CIGというコドンはCGGと見なされRとして翻訳される（本文参照）．

が，どのようにCa^{2+}透過性が制御されているかは少しずつ解明されている．

AMPA受容体は，4種のサブユニット（GluR1-GluR4）の単独または様々な組み合わせからなる4量体である．各サブユニットは共通構造をもち，相互に約70%のアミノ酸配列の相同性をもち，細胞外のN端，膜ドメイン（M1～M4），細胞内のC端からなる（図1）[2,3,16-20]．AMPA受容体

のCa^{2+}透過性を決定する因子には，1) GluR2サブユニット，2) GluR2サブユニットのRNA編集（特にQ/R部位），3) flip/flop splicing variantやR/G部位の編集率などチャネルの開口を編集するドメインがあり，細胞全体としては[4]細胞表面のAMPA受容体密度もCa^{2+}流入量を決定する大きな因子となる．しかし，これらの因子のすべてが細胞死に直接関連するわけではなく，AMPA受容体仮説には後述するように1)と2)のかかわりが大きい．

第一にチャネルのCa^{2+}透過性決定に重要な役割をはたしているのはGluR2サブユニットである．AMPA受容体を構成する4つのサブユニットのうちGluR2を含む受容体は，Ca^{2+}透過性が低く，GluR2を含まないGluR1，3，4のサブユニットだけで構成された受容体は，高いCa^{2+}透過性を示す[21-23]．

つまりAMPA受容体のCa^{2+}透過性は，GluR2の有無により決定される．たとえば，ラット小脳プルキニエ細胞や海馬錐体細胞などでは，他のサブユニットに比べGluR2が多く発現し，AMPA受容体のCa^{2+}透過性は低く[24]，海馬のバスケット細胞，新皮質の非錐体細胞，小脳のBergmannグリア細胞などではGluR2サブユニットがほとんど発現していないため，Ca^{2+}透過性は高い[25]ことが知られている．

第二にAMPA受容体の各サブユニットのM2にあるQ/R部位がCa^{2+}透過性を制御している．Q/R部位がCa^{2+}透過性決定に重要なのはチャネル・ポアに面しており，陽電化のRがCa^{2+}を弾くのに対して電気的に中性のQではこの作用が弱いためであると考えられている．同部位はGluR2以外ではグルタミン（Q）であるのに対して，GluR2だけはアルギニン（R）である（図1）．しかしゲノムレベルでは，GluR2も他のサブユニット同様にQをコードしている．どうしてRになるのかというと，RNA編集という現象が起こるためである．つまり，DNAからRNAへ転写後，mRNAになる前に，adenosine deaminase acting on RNA type 2（以下ADAR2）とよばれる編集酵素により，アデノシン（A）からイノシン（I）へとRNA編集が起こることで塩基置換され，リボソームでIはグアノシン（G）と同等であると見なされるため，CIGというコドンはCGGと見なされRとして翻訳される[26]．未編集型GluR2（Q）は他のサブユニット同様AMPA受容体のCa^{2+}透過性を制御できないので，編集型GluR2（R）を含んだAMPA受容体の割合が減少する，あるいは未編集型GluR2（Q）を含んだAMPA受容体の割合が増加すると細胞内へのCa^{2+}流入が高まる[27]．RNA編集は，GluR2 Q/R部位以外にもカイニン酸受容体サブユニットであるGluR5，GluR6のQ/R部位やGluR2，GluR3，GluR4サブユニットのR/G部位，Kv1.1 I/V部位，$5HT_{2c}$ A～E部位ではRNA編集の有無によりチャネル特性に変化が生じ，ADAR2のself-editingではスプライシングサイトの変化によるフレームシフトにより，酵素活性が変化する[28]など様々なRNAのそれも複数の部位で生じているが，その編集率は一定せず様々である．ところが，GluR2のQ/R部位は，胎生期から成熟期に至るまでほぼ100%編集されている[29]という点で特異的であり，他には見いだされていない．

しかし，GluR2のノックアウトマウスでは細胞死が生じず[30]，一方でRNA編集を阻止したmutant mouseはGluR2 Q/R部位が0.1%以下に低下し，生後20日以内に痙攣重積により死亡する[31]ことなどからGluR2のRNA編集にはQ/R部位の電荷状態の制御以外にも，AMPA受容体の機能を修飾する作用があると考えられ，生存を左右するほど生物学的にもきわめて重要な意味をもっていると推測される．

その修飾作用の一つが，ニューロン表面のAMPA受容体密度，サブユニット会合効率への

関与である．GregerらはQ/R部位がQかRであるかによってサブユニットの会合確率が変わり，特に4量体形成において主な要因となること，すなわち，未編集型GluR2（Q）は編集型GluR2（R）よりも効率的に機能的AMPA受容体を形成しやすいことを示した[32]．さらにQ/R部位のアミノ酸残基の違いによりtrafficking効率が異なり，Q型（GluR1, 3, 4, 未編集GluR2（Q））はR型（編集型GluR2（R））に比し効率が高いこと，すなわち未編集型GluR2（Q）が存在する場合には編集型GluR2（R）が小胞体から輸送されにくいのに対して，GluR2（Q）を含むサブユニット複合体は，効率よく膜表面にtraffickingされることを示した[33]．以上のようにQ/R部位がQであるかRであるかによってサブユニットの会合確率およびtrafficking効率が異なり，結果的にGluR2の細胞膜表面へのtrafficking効率は，編集型GluR2（R）より未編集型GluR2（Q）のほうがはるかに高くなる．すなわち，GluR2ノックアウトマウスには細胞死が起こらないのに，RNA編集異常マウスで痙攣重積が起こるのは，RNA編集の障害の方が細胞表面のCa^{2+}透過性AMPA受容体密度が高く，細胞内Ca^{2+}濃度の上昇もより大きいので神経細胞死が起こると考えられる．培養細胞では，未編集型GluR2発現させても，traffickingを阻止すると神経細胞死も阻止される[34]．

C. AMPA受容体サブユニット発現とALSの運動ニューロン死

これらの結果を踏まえ，神経細胞死に関連する分子変化であるGluR2の減少（Ca^{2+}透過性AMPA受容体の割合の増加）ないしGluR2 Q/R部位の編集率低下（Ca^{2+}透過性AMPA受容体の実質的増加）の有無をALSの運動ニューロンで検討するためにKwakらはlaser microdissectorを用いて凍結割検組織から単一神経細胞を切り出し，孤発性ALS脊髄運動ニューロンの単一神経細胞レベルの検討において，GluR2 mRNA発現量に有意な減少がないこと[35]，および脊髄前角組織レベルで，すでに報告していた[36]部位選択的・疾患特異的なGluR2 Q/R部位の編集率低下を確認した[1]．図2に示すように，正常対照群の運動ニューロンでは，全例GluR2 Q/R部位は100% RNA編集されていたが，ALS群では0～100%とばらつき，平均値は38～75%と低下していた．ALS群における小脳プルキンエ細胞の編集率は，正常対照群と同様にほぼ100%に保たれていた．また，他の神経変性疾患の同細胞を検索したが，編集率は正常対照と同様のレベルによく保たれていた．さらに症例数を増やし，孤発性ALSと診断された症例で，古典型，PBP，ALS-D，好塩基性封入体が出現する若年発症例[37]について編集率を調べたところ臨床像の異なるこれらのALSでも編集率は低下しており，共通の分子異常が発症のメカニズムにあることが推測される[38]．一方でSOD1関連性家族性ALS（ALS1）モデルラットやSBMA（球脊髄性筋萎縮症）の運動ニューロンでは同部位の編集率はコントロールと同様であり[39]，これらの疾患の運動ニューロンでは孤発性ALSとは異なる細胞死のメカニズムが働いていると考えられる．一方で，変異*SOD1*トランスジェニックマウスでは，AMPA受容体を介した神経細胞死が働いていることが，GluR2欠損マウスとの交配による興奮毒性の増強[40]やCa^{2+}を透過するQ/R部位を人工的なGluR2〔GluR-B（N），N（アスパラギン）〕を導入した変異マウスと変異*SOD1*遺伝子のdouble transgenicマウスにおける神経細胞死の促進[41]から示されている．ALS1でGluR2のRNA編集が正常だとすると，GluR2の欠乏によるAMPA受容体のCa^{2+}透過性亢進が予想されるが，GluR2の過剰発現により生存期間が延長することを示した報告[42]，GluR3の発現量が増加しているとする

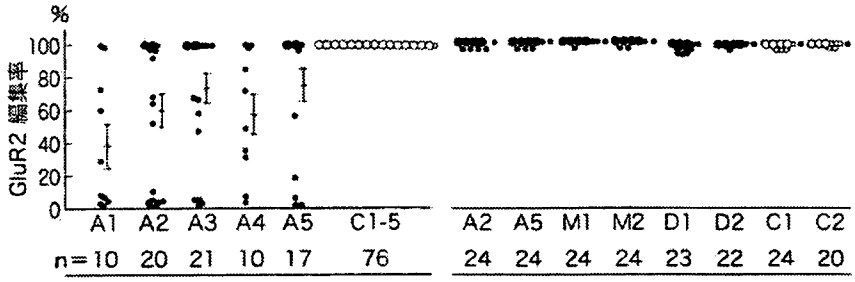

図2　単一神経細胞におけるGluR2 Q/R部位RNA編集率（文献1より改変）
各点（大きな点は5細胞，小さな点は1細胞）は，ALS群5例（A1-A5），コントロール群5例（C1-C5）の単一脊髄運動ニューロンにおけるGluR2 Q/R部位のRNA編集率と，ALS群2例（A2，A5），multiple system atrophy（以下MSA，多系統萎縮症）群2例（M1，M2），dentatorubral-pallidoluysian atrophy（以下DRPLA，歯状核赤核淡蒼球ルイ体萎縮症）群2例（D1，D2），コントロール群2例（C1，C2）の単一小脳プルキンエ細胞の編集率を表している．平均値± 標準誤差と解析した細胞数（n）も示した．運動ニューロンにおける正常コントロール76個の内訳は，C1; 28，C2; 12，C3; 13，C4; 12，C5; 11である．運動ニューロンでは，正常コントロール群のすべての細胞において，例外なく編集率は100%であった．これに対して，ALS群では，解析した5ケースすべてにおいて，編集率は運動ニューロンごとに0%から100%まで大きくばらつき，平均値も正常コントロール群と比較し，有意に低下していた（Mann-Whitney U test，$p<0.001$）．一方，小脳プルキンエ細胞における編集率については，ALS群，MSA群，DRPLA群とコントロール群の間には有意差はない（Mann-Whitney U-test，$p>0.05$）．

報告[43,44]は，この予測を支持する．特に，GluR3の発現量増加は，我々がカイニン酸を長期髄注することにより作成したALSのモデルラットにもみられる分子変化であり[45]，変異SOD1トランスジェニックマウス，家族性ALS1ではAMPA受容体の持続的刺激により運動ニューロンの興奮性が高まった結果，相対的にGluR2の割合が下がることでAMPA受容体のCa^{2+}透過性が亢進し，細胞死に至るカスケードにつながることが予想される．このように，ALS1と，痴呆を伴うALSを含む孤発性ALSとでは，神経細胞死を引き起こす分子メカニズムが異なることは，ALS，前頭側頭型痴呆（FTLD）の細胞内封入体に特異的に集積することが示されているTDP-43が，ALS1には見いだされていない[46,47]ことからきわめて興味深い．他方，アンドロゲン受容体のCAGリピートが伸長しているSBMAでは，同じポリグルタミン病であるHuntington病モデルマウスでの検討から[48-51]，AMPA受容体を介した神経細胞死は働いていないと考えられる．このように運動ニューロン疾患の神経細胞死には図3に示すように，異なる複数の分子メカニズムが独立に働き，ALSにはAMPA受容体を介する運動ニューロン死が働いているものの単一の分子メカニズムではないことが推測される[52]．

以上から，孤発性ALS脊髄運動ニューロンで認められたRNA編集異常は，細胞選択的かつ疾患特異的な分子変化であり，神経細胞死に直接かかわっている可能性が高いと考えられる．このような選択性・特異性を生む機序としては，脊髄運動ニューロンのAMPA受容体総mRNA発現量およびGluR2サブユニットのAMPA受容体サブユ